Air Force Institute of Technology
AFIT Scholar

Theses and Dissertations | Student Graduate Works

3-14-2014

An Assessment of Normalized Difference Skin Index Robustness in Aquatic Environments

Alice W. Chan

Follow this and additional works at: https://scholar.afit.edu/etd

Recommended Citation
Chan, Alice W., "An Assessment of Normalized Difference Skin Index Robustness in Aquatic Environments" (2014). *Theses and Dissertations*. 592.
https://scholar.afit.edu/etd/592

This Thesis is brought to you for free and open access by the Student Graduate Works at AFIT Scholar. It has been accepted for inclusion in Theses and Dissertations by an authorized administrator of AFIT Scholar. For more information, please contact richard.mansfield@afit.edu.

AN ASSESSMENT OF NORMALIZED DIFFERENCE SKIN INDEX ROBUSTNESS IN AQUATIC ENVIRONMENTS

THESIS

Alice W. Chan, First Lieutenant, USAF

AFIT-ENG-14-M-17

DEPARTMENT OF THE AIR FORCE
AIR UNIVERSITY

AIR FORCE INSTITUTE OF TECHNOLOGY

Wright-Patterson Air Force Base, Ohio

DISTRIBUTION STATEMENT A:
APPROVED FOR PUBLIC RELEASE; DISTRIBUTION UNLIMITED

The views expressed in this thesis are those of the author and do not reflect the official policy or position of the United States Air Force, the Department of Defense, or the United States Government.

This material is declared a work of the U.S. Government and is not subject to copyright protection in the United States.

AFIT-ENG-14-M-17

AN ASSESSMENT OF NORMALIZED DIFFERENCE SKIN INDEX ROBUSTNESS IN AQUATIC ENVIRONMENTS

THESIS

Presented to the Faculty

Department of Electrical and Computer Engineering

Graduate School of Engineering and Management

Air Force Institute of Technology

Air University

Air Education and Training Command

in Partial Fulfillment of the Requirements for the

Degree of Master of Science in Electrical Engineering

Alice W. Chan, BSEE

First Lieutenant, USAF

March 2014

DISTRIBUTION STATEMENT A:
APPROVED FOR PUBLIC RELEASE; DISTRIBUTION UNLIMITED

AFIT-ENG-14-M-17

AN ASSESSMENT OF NORMALIZED DIFFERENCE SKIN INDEX ROBUSTNESS IN AQUATIC ENVIRONMENTS

Alice W. Chan, BSEE
First Lieutenant, USAF

Approved:

/signed/	12 Mar 2014
Lt Col Jeffrey D. Clark, PhD (Chairman)	Date
/signed/	12 Mar 2014
Dr. Stephen C. Cain (Member)	Date
/signed/	12 Mar 2014
Col Matthew D. Sambora, PhD (Member)	Date

AFIT-ENG-14-M-17

Abstract

The Normalized Difference Skin Index (NDSI) is a numeric value generated from two wavelengths of the electromagnetic spectrum, a feature that can be utilized for a dismount detection system. Skin is a major anatomical trait of human beings, furthermore, the most exposed trait to the elements. An aspect of a person's skin is typically uncovered, such as their face or hands. If skin pixels are detected in a spectral image, we can confidently conclude a person is present in the scene.

There has been successful research on the use of spectral imagery for NDSI skin detection in ideal conditions [35]. However, in efforts to achieve an operational dismount detection system, the robustness of NDSI has to be explored for more austere conditions. The focus of this thesis is on aquatic environments.

Water in aquatic environments poses a challenging problem in the spectral domain because of its absorptive characteristic in several regions of the electromagnetic spectrum, known as water absorption bands [13, 15]. In these particular bands, spectral information becomes occluded from the "dominance" of water. Unfortunately, the two NDSI wavelengths exist in close proximity with these bands.

Experiments were devised to emulate scenarios that may arise between skin and water in a pixel of a hyperspectral image. With a mixed pixel of skin with water in the background, the spread of NDSI values were within a range defined by previous research until 64% or less of the pixel constituted skin. With a mixed pixel of skin with water droplets, the evaluated amount of water had negligible impact on NDSI. A mixed pixel of skin under a thin layer of water rendered NDSI useless with a shallow depth of 5 mm; water layers prove to be extremely detrimental to NDSI. Also, the temporal factor of water absorption by skin was assessed. Within the evaluated durations, up to 6300 s, the results showed negligible impact on NDSI.

The following pages would not exist without the support my family and friends.
Thank You.

Acknowledgments

First and foremost, I need to personally acknowledge Lt Col Jeffrey Clark, my advisor. Without his guidance, who knows where I would have ended up. Thank you.

To the good folks of AFIT/SERG, thank you for the assistance and keeping me sane in the laboratory.

Alice W. Chan

Table of Contents

Page

Abstract . . . iv

Dedication . . . v

Acknowledgments . . . vi

Table of Contents . . . vii

List of Figures . . . viii

List of Abbreviations . . . ix

I. Introduction . . . 1

1.1 Dismount Detection . . . 1
1.2 Previous Work . . . 2
1.3 Motivation . . . 3
1.4 Challenges . . . 4
1.5 Problem Statement . . . 6
1.6 Approach . . . 6
1.7 Thesis Overview . . . 6

II. Background . . . 8

2.1 Human Skin . . . 8
2.1.1 Anatomy [21] . . . 8
2.1.2 Thickness . . . 10
2.1.3 Color . . . 10
2.1.4 Water and Skin . . . 10
2.2 Spectroscopy . . . 11
2.2.1 Radiative Transfer Model . . . 11
2.2.2 Atmosphere and Illumination . . . 11
2.2.3 Water and Absorption Bands . . . 13
2.3 Spectral Signature of Skin . . . 14
2.4 NDSI . . . 18
2.5 Chapter Summary . . . 19

Page

III. Methodology 20

3.1 Data Acquisition System 20
3.1.1 Operations [28] 21
3.1.2 Field-Of-View 21
3.1.3 Calibration 22
3.2 Experiment Configurations 26
3.3 Water 29
3.4 Skin Percentage Extraction 29
3.5 Data Processing 31
3.6 Chapter Summary 31

IV. Results 32

4.1 Experiment 1 - Water Background 32
4.1.1 Data Collection 32
4.1.2 NDSI Evaluation 35
4.2 Experiment 2 - Water Droplets 41
4.2.1 Data Collection 41
4.2.2 NDSI Evaluation 41
4.3 Experiment 3 - Water Layer 46
4.3.1 Data Collection 46
4.3.2 NDSI Evaluation 46
4.4 Experiment 4 - Waterlogged Skin 50
4.4.1 Data Collection 50
4.4.2 NDSI Evaluation 50
4.5 Chapter Summary 56

V. Conclusion 57

5.1 Thesis Summary 57
5.2 Future Work 59

Appendix: Water Background Data Sets 61

Appendix: Cloth Background Data Sets 64

Appendix: Sand Background Data Sets 66

Appendix: Grass Background Data Sets 69

Page

Bibliography 72

List of Figures

Figure Page

1.1 A demonstration of NDSI for skin detection; (a) Hyperspectral image (in color) featuring people with various skin color and confusers; (b) Truth mask for the skin pixels; (c) A large NDSI threshold results in higher probability of detection and false detection; (d) A smaller NDSI threshold results in lower probability of detection and false detection. [6] 4

1.2 Hypothetical aquatic environment scenario demonstrating five possible mixed pixels: (a) all water, (b) all skin, (c) skin overlaid with water, (d) non-overlapping skin and water, and (e) skin under water. 5

2.1 Cross-section view of a human skin model illustrating the complex structure made of multiple components and the three distinct layers: epidermis, dermis, and subcutaneouos tissue [5]. 9

2.2 The sensor-reaching radiation could come from other sources, besides reflectance from the target. Five possible paths of travel are illustrated. 12

2.3 The sensor-reaching radiation of the Sun, measured from the ground on a bright and cloudless day. The local minimums demonstrates the influence of atmosphere from absorption and scattering. The two vertical red lines mark the two NDSI wavelength at 1080 nm and 1580 nm. 13

2.4 Absorption spectrum of liquid and ice water. Major water absorption bands exist at 1500 nm, 1900 nm, and 2500 nm. [22] The two vertical red lines mark the two NDSI wavelength at 1080 nm and 1580 nm. Water absorption may pose a problem to the latter NDSI wavelength. 14

Figure Page

2.5 Spectral signature of human skin. The two vertical red lines mark the two NDSI wavelength at 1080 nm and 1580 nm. The wavelengths were chosen to correspond to a local maximum and a local minimum [35]. 15

2.6 The absorption coefficient of water (blue), hemoglobin (pink), and melanin (black), the major components used to model skin [16]. The two vertical red lines mark the two NDSI wavelength at 1080 nm and 1580 nm. 16

2.7 The spectral reflectance of skin for two skin colors, light (blue line) and dark-brown (black line). Darker skin has more melinan, which is apparent in the plot from the lower reflectance in the visible region. The two vertical red lines mark the two NDSI wavelength at 1080 nm and 1580 nm. 17

3.1 The ASD FieldSpec® 3 spectroradiometer attached to the ASD contact probe. The computer is for the software that controls the FieldSpec. 20

3.2 Parameters that define the FieldSpec's field-of-view: Y is the diameter of the field-of-view, D is the effective diameter of the foreoptic lens, X is the distance to the target, and A is the foreoptic angular field-of-view [28]. 22

3.3 An image of the three white reference panels used in the experiments. 23

3.4 Screenshots of RS^3, the ASD software used to operator the FieldSpec. On start up, the ASD has to be optimized and calibrated for reflectance measurements and dark current subtraction; (a) The display after proper optimization, there should be a reading for across the whole spectrum of 350 nm to 2500 nm; (b) The display after dark current subtraction and white reflectance. 25

3.5 The mixed pixel configuration. The major equipment used in this configuration and the target area are highlighted in yellow. 27

3.6 The configuration for mixed pixel experiments featuring the pistol grip and the two illumination lamps; (a) Side view of the set up; (b) Side and top-down view of the target area where Y is the diameter of the field-of-view. 28

3.7 Screenshots of the skin percentage extraction process using ImageJ, a image processing software; (a) The black markers define the boundary of the field-of-view. A circular selection tool is used to select the area; (b) Measurement of the selected field-of-view circle; (c) An image of a mixed pixel with the field-of-view mask applied; (b) A manual selection tool is used to select the skin in the field-of-mask for measurement. 30

4.1 An image highlighting the two areas human skin samples were collected from in the experiments. For Experiment 1 and 3, area (a) was used. For Experiment 2 and 4, area (b) was used. 33

4.2 Histogram of the data set from Experiment 1 (Water Background). An even distribution of data is collected of various skin percentages. 34

4.3 NDSIs of the data set from Experiment 1 (Water Background). The error bars denotes the standard deviation. The red line is a linear fitted line for reference. There is a wide spread in the range of NDSI values for skin-positive mixed pixels. A 100% skin pixel has a NDSI of approximately 0.7, while a 10% skin pixel has a NDSI of appropriately 0.85. 35

4.4 The spectral reflectance of a mixed pixel of skin with water in the background at %100 skin (black), 0% skin (blue), 50% skin (green), and the theoretical linear mixing model of 50% skin (dashed). The mixed pixels from Experiment 1 does not fit a linear mixing model, or else the green and dashed lines would overlap. 37

Figure Page

4.5 An image captured in Experiment 1 from the optical camera suspended above the set up configuration. Shadows are casted by the hand due to the angle of the illumination source. These shadows influences the measured reflectance spectrum. 38

4.6 The NDSIs of the data set from Experiment 1 using other background materials: (a) cloth, (b) sand, and (c) grass. The error bars denotes the standard deviation. The red line is a linear fitted linear for reference. NDSI values increases as skin percentage increase, unlike the water background. 40

4.7 Histogram of the data set from Experiment 2 (Water Droplets). Samples more than 5 mL of water droplets are not taken due to practicality; because with additional water, the droplets rolls off the back of the hand. The collection at 35 mL resulted in a loss of over 50% water droplets. 42

4.8 NDSIs of the data set from Experiment 2 (Water Droplet). The error bars denotes the standard deviation. NDSI is mostly invariant to water droplets with a small range of NDSI values for skin-positive pixels. 43

4.9 The reflectance spectra of the data set with mixed pixels of skin with water droplets; (a) Minimal variation between the spectra is apparent from a view of the full spectrum range; (b) An enlargement of the band around 1080 nm; (c) An enlargement of the band around 1580 nm. Note the inconsistent order of the reflectance between (b) and (c). The nonlinear effect of water at those two wavelengths is seen from the different changes in range. 45

4.10 Histogram of the data set from Experiment 3 (Water Layers). 47

4.11 NDSIs of the data set from Experiment 2 (Water Layers). The error bars denotes the standard deviation. The NDSI of 0.74 at 0 mm is for the case of no water. Once 5 mm or more water is added, NDSI fails to function due to the lost of the second wavelength, 1580 nm, from water absorption. 48

4.12 The reflectance spectra of the data set with mixed pixels of skin under a water layers. Past 1400 nm, water absorption is strong enough to occult skin reflectance, including the second NDSI wavelength, 1580 nm. 49

4.13 Histogram of the data set from Experiment 4 (Waterlogged Skin). 51

4.14 NDSIs of the data set from Experiment 4 (Waterlogged Skin). The error bars denotes the standard deviation. The red line is a linear fitted line for reference. There is not a consistent pattern between time duration and NDSI. Overall, NDSI remain relatively constant around 0.72 and invariant to the temporal affect of waterlogged skin. 53

4.15 The reflectance spectra of the data set with waterlogged skin; (a) Minimal variation between the spectra is apparent from a view of the full spectrum range except in band around 800 nm and 1080 nm; (b) An enlargement of the band around 1080 nm; (c) An enlargement of the band around 1580 nm. Note the inconsistent order of the reflectance between (b) and (c). The nonlinear effect of water at those two wavelengths is seen from the different changes in range. . 54

4.16 A method for hydration calculation [2]. The area under the spectrum in the region of 960 nm to 1700 nm is plotted against time duration. The premise of this method is that more water meaning a lower reflectance, which results in a smaller area. The area remains relatively constant across the time duration; either this method does not work or an insignificant amount of water is absopred by skin. 55

Figure Page

A.1 The average spectral reflectance of the (a) 0% skin and (b) 100% skin samples of Experiment 1. 61

A.2 The average spectral reflectance of samples from of Experiment 1 compared to a linear mixing model (a) 10% and (b) 20%. 61

A.3 The average spectral reflectance of samples from of Experiment 1 compared to a linear mixing model (a) 30% and (b) 40%. 62

A.4 The average spectral reflectance of samples from of Experiment 1 compared to a linear mixing model (a) 50% and (b) 60%. 62

A.5 The average spectral reflectance of samples from of Experiment 1 compared to a linear mixing model (a) 70% and (b) 80%. 63

A.6 The average spectral reflectance of samples from of Experiment 1 compared to a linear mixing model 90%. 63

B.1 A data set of reflectance spectra is created from mixed pixels of skin with cloth in the background; (a) Histogram of data set; (b) NDSI of the data set. 64

B.2 Three averaged reflectance spectra from the Cloth Background data set: 100% skin (black), 100% cloth (blue), 50% skin (dashed). 64

B.3 The average spectral reflectance of samples from of Experiment 1 with cloth background; (a) 13.5% (b) 23% (c) 36% (d) 41% (e) 65% (f) 100% 65

C.1 A data set of reflectance spectra is created from mixed pixels of skin with sand in the background; (a) Histogram of data set; (b) NDSI of the data set. 66

C.2 Three averaged reflectance spectra from the Sand Background data set: 100% skin (black), 100% sand (blue), 50% skin (dashed). 66

C.3 The average spectral reflectance of samples from of Experiment 1 with sand background; (a) 16% (b) 21% (c) 30% (d) 40% (e) 50% (f) 58% 67

Figure Page

C.4 The average spectral reflectance of samples from of Experiment 1 with sand background; (a) 70% (b) 80% (c) 92% 68

D.1 A data set of reflectance spectra is created from mixed pixels of skin with grass in the background; (a) Histogram of data set; (b) NDSI of the data set. 69

D.2 Three averaged reflectance spectra from the Grass Background data set: 100% skin (black), 100% grass (blue), 50% skin (dashed). 69

D.3 The average spectral reflectance of samples from of Experiment 1 with grass background; (a) 10% (b) 24% (c) 40% (d) 55% (e) 68% (f) 80% 70

D.4 The average spectral reflectance of samples from of Experiment 1 with grass background; (a) 100% 71

List of Abbreviations

Abbreviation	Definition
AFIT	Air Force Institute of Technology
ASD	Analytical Spectral Devices
ISIS	Integrated Surveillance Intelligence System
NDGRI	Normalized Difference Green Red Index
NDSI	Normalized Difference Skin Index
NDVI	Normalized Difference Vegetation Index
NIR	Near-Infrared
SAR	Search and Rescue
SERG	Sensors Exploitation Research Group
SWIR	Short-Wavelength Infrared
US	United States
USAF	United States Air Force
VIS	Visible
VNIR	Visible Near Infrared

AN ASSESSMENT OF NORMALIZED DIFFERENCE SKIN INDEX ROBUSTNESS IN AQUATIC ENVIRONMENTS

I. Introduction

1.1 Dismount Detection

Dismount detection is a field of research dedicated to exploring techniques to automate people detection; specifically, people on the ground and outside of any structures, e.g. vehicles or buildings. The goal of automation is to minimize the man-in-the-loop through the development of an dependable artificial intelligent agent. In regard to the dismount detection system, the objective is to replace the human operator for functions that involve locating a dismount. Consider the following application examples of the dismount detection system in search and rescues (SAR) and surveillance.

Time is vital when searching for a missing person; in an instance with a dementia patient, there is a 25% fatality rate if the person is missing for longer than 24 hours [29]. However, conventional SAR operations still utilize antiquated techniques. The standard operating procedure consists of defining a probable area and deploying search teams into that area [29]. This process can quickly become time consuming depending on a wide range of problematic factors: search area size, available personnel, terrain, time of day, etc. In place of the search teams, an airborne dismount detection system can be fielded with the capability of covering a larger area, at a greater speed, also, completely avoiding a number of problematic factors.

Most surveillance systems depend on the active engagement of human operators to monitor a screen, in search of unusual and suspicious targets. In such systems, success or failure relies on the operator. Studies have been performed to understand the relationship

between stress and fatigue with work associated with video display terminals and visual-based tasks [33, 41]. While causation is inconclusive, stress and fatigue have been proven to exist. An affected operator will have degraded performance and missing a target could have drastic consequence. In place of the human operator, a dismount detection system will function without issues such as stress and fatigue.

A report, issued by the United States (US) Department of Homeland Security in 2005, evaluated the effectiveness of one such surveillance system. The Integrated Surveillance Intelligence System (ISIS) consists of a network of sensors: daylight cameras, infrared cameras, seismic sensors, and magnetic sensors, placed along the US border. The system was implemented as a force-multiplication measure; with over 6000 miles to cover and limited staff resource, technology has to be leveraged to effectively monitor this expansive area. The results from the report concluded that this measure was not realized with ISIS. Two major limitations of the system are mentioned in the report. One, the cameras can not automatically detect activity and movement. Two, the ISIS depends on a staff with limited availability and capability to function. If ISIS could be upgraded with a dismount detection system, these concerns could be alleviated. [30]

1.2 Previous Work

Local to the Air Force Institute of Technology (AFIT), at Wright-Patterson Air Force Base, is a consortium known as the Sensors Exploitation Research Group (SERG). The primary mission of SERG is to conduct research that enhances war-fighter capabilities through application of artificial intelligence and sensor technology. Dismount detection is an active area of interest of the research group. In recent years, a wide range of research has been conducted by SERG and AFIT related to the topic. Examples of the work include:

- Spectral detection of human skin in visible and short-wavelength infrared hyperspectral imagery with radiometric calibration [3],

- Improved multispectral skin detection and its application to search space reduction for dismount detection based on histograms of oriented gradients [6],
- Distributed spacing stochastic feature selection and its application to textile classification [7],
- Dismount threat recognition through automatic pose identification [11],
- A physical model of human skin and its application for search and rescue [35].

The work accomplished by Nunez established the foundation for the skin detection research conducted by SERG, resulting in the Normalized Difference Skin Index (NDSI). NDSI utilizes two different wavelengths of the electromagnetic spectrum, one in the near-infrared (NIR) and the other in the short-wavelength infrared (SWIR) regions, to create a feature for human skin detection. [35]

The NDSI algorithm has shown positive results as a method for skin detection in ”ideal” conditions, such as the bright and cloudless day shown in Figure 1.1. However, to be implemented in a fully operation system, it must be capable of accomplishing its objective in more austere conditions. Fully understanding the capabilities and limitation of any new technology is necessary in furthering its development.

1.3 Motivation

Water is an indispensable resource and an essential component for human life [14]. Given the world population, studies have shown that 50% of all people live within 3000 m of a body of freshwater. Combined with the fact that approximately 70% of the Earth's surface is covered by water, there are high probabilities that a dismount of interest will be found in an aquatic environment [1]. We must therefore create a dismount detection system that operates without limitation in water.

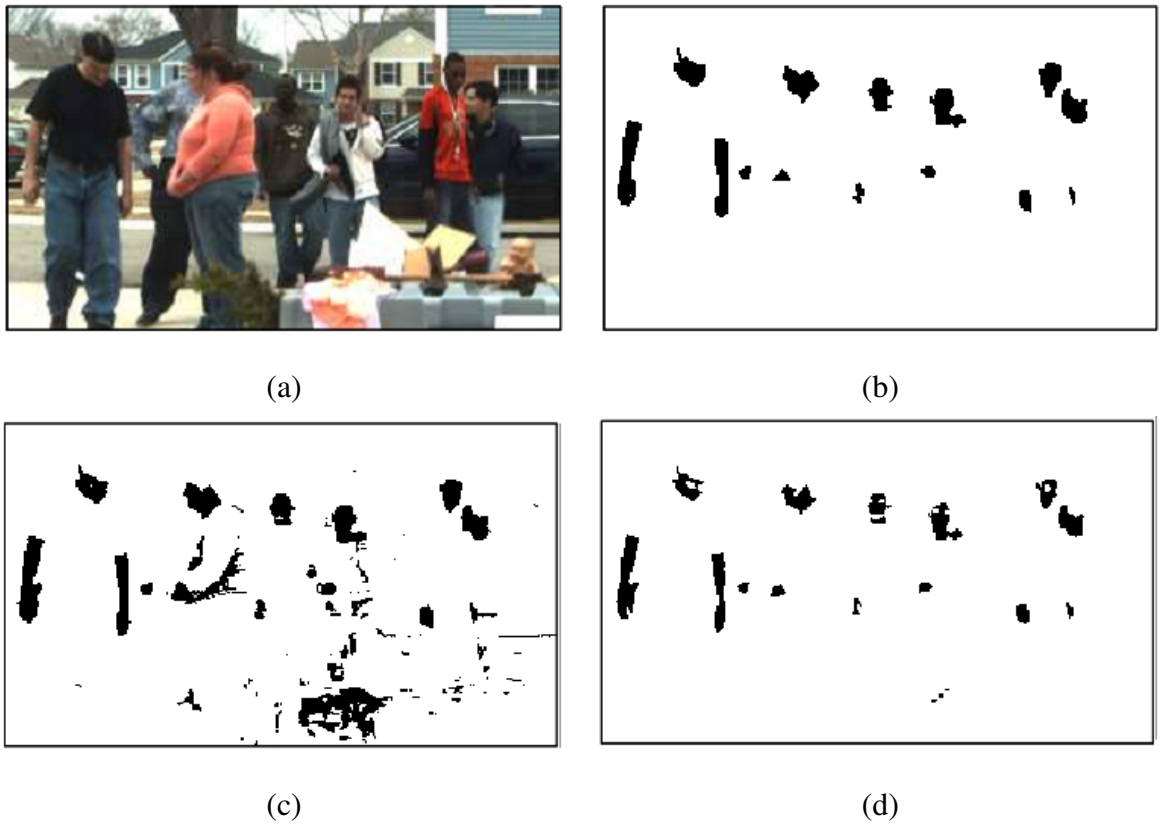

Figure 1.1: A demonstration of NDSI for skin detection; (a) Hyperspectral image (in color) featuring people with various skin color and confusers; (b) Truth mask for the skin pixels; (c) A large NDSI threshold results in higher probability of detection and false detection; (d) A smaller NDSI threshold results in lower probability of detection and false detection. [6]

1.4 Challenges

Presented with the hyperspectral image of the scenario illustrated in Figure 1.2, five possible mixed pixel scenarios may arise between the interaction of skin and water: (a) all water, (b) all skin, (c) skin overlaid with water, (d) non-overlapping skin and water, and (e) skin under water.

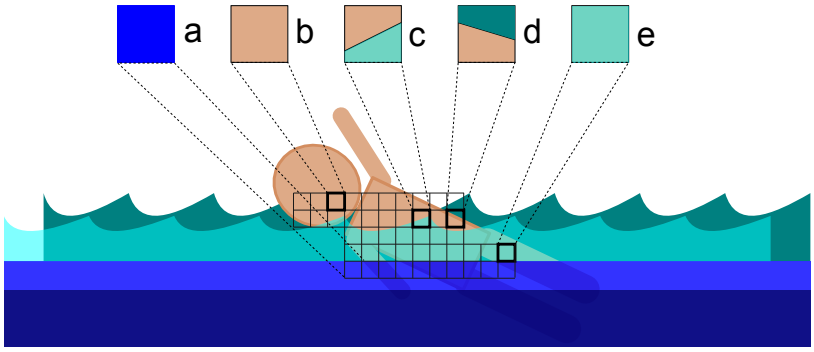

Figure 1.2: Hypothetical aquatic environment scenario demonstrating five possible mixed pixels: (a) all water, (b) all skin, (c) skin overlaid with water, (d) non-overlapping skin and water, and (e) skin under water.

The first scenario, (a) all water, is trivial with no skin present. The second scenario, (b) all skin, should not pose a challenge based on the results of the work conducted by the SERG in Section 1.2. The last three instances are the focus of this thesis.

Depending on multiple factors, such as the spatial resolution of the sensor given the target-sensor distance, a pixel from a image may not be entirely composed of a single material. With spectral sensors, the measured spectrum of a ”mixed pixel” represents an average of the material in the pixel as a function of each material’s abundance, a concept known as a linear mixing model. [18] However, if the materials are laid out in a complex distribution, a nonlinear model is more appropriate [19]. The variation between (c), (d), and (e) of Figure 1.2 goes to demonstrate how singular the distribution between the materials can be. Given a mixed pixel with skin present, NDSI may still fail. The relation between the two NDSI wavelengths is the crux of this skin detection technique. The problem posed by water is that its presence will change the spectrum measured by the sensor, including those two wavelengths. The evaluation of NDSI robustness, at the challenge of water, becomes not a question of if but instead: how?

In addition to the issue of spectral mixing, water is also capable of altering skin physically. Most people have witnessed some aspect of this phenomenon in the form of pruney fingers after a hot shower. The degree of change, spectrally, will be examined in this thesis.

1.5 Problem Statement

The goal of this thesis is to evaluate how robust NDSI is in aquatic environments. Specifically, the following four questions are formed based on the challenges proposed in the previous section.

1. Water Background. How does a mixed pixel of skin with water in the background impact NDSI?

2. Water Droplets. How does a mixed pixel of skin with water droplets on surface of the skin impact NDSI?

3. Water Layer. How does a mixed pixel of skin under a thin layer of water impact NDSI?

4. Waterlogged Skin. How does skin that has been submerged in water impact NDSI?

1.6 Approach

An experimental approach is taken to complete this thesis. In order to evaluate the impact of water on NDSI, with respect to the four questions posed in Section 1.5, data sets for the scenario from Figure 1.2 were created in a laboratory setting.

1.7 Thesis Overview

Chapter II covers background information and contains summaries of findings from the literature review that was conducted. Chapter III discusses the methodology behind the experiments that were performed and details how the data was collected. Chapter IV contains the results of the experiments and an assessment of the NDSI. A summary and

conclusion of this thesis is presented along with proposed future avenue of research in Chapter V.

II. Background

2.1 Human Skin

Skin is an organ of the human body that performs multiple functions essential to life sustainment [24]. A few of these functions include: serving as the physical layer between the environment and the internal organs, regulation of body temperature, and maintaining hydration [17, 21, 24]. The skin is a complex non-homogeneous structure that varies drastically from person to person. A cross-section of skin, shown in Figure 2.1, illustrates three distinct layers (epidermis, dermis, and subcutaneous tissue) and multiple other components [21].

2.1.1 Anatomy [21].

The skin is structurally organized into three layers: epidermis, dermis, and subcutaneous tissue. The outermost layer of the skin, the epidermis, is further stratied into five different sub-layers: stratum corneum, stratum licidum, stratum granulosum, stratum spinosum, and stratum basale. Keratinocytes cells make up the majority of the epidermis. Through keratinization, keratinocytes originate in the stratum basale layer and travel to the top most stratum corneum layer. Each sub-layer of the epidermis is defined by a phase of the keratinization process. Below the epidermis is the dermis, the thickest layer of the skin. The dermis is divided into two different sub-layers, the papillary and reticular layer. Connective tissues made up of reticulum fibers, elastic fibers, and collagen forms this layer. Major components of the skin also resides in the dermis, such as: blood vessels, capillaries nerve ending, sweat glands, and hair follicles. Subcutaneous tissue lies below the dermis and constitutes most of the body's fat storage.

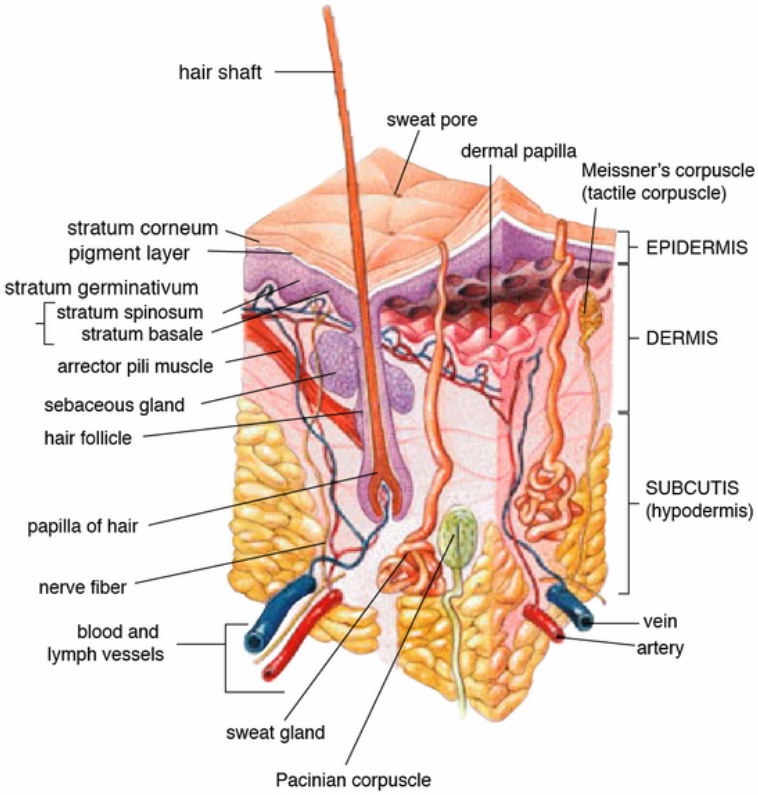

Figure 2.1: Cross-section view of a human skin model illustrating the complex structure made of multiple components and the three distinct layers: epidermis, dermis, and subcutaneouos tissue [5].

2.1.2 Thickness.

A collection of skin samples may vary drastically in thickness, despite measurements taken from a single subject. Studies have shown that multiple factors influence the diversity in skin thickness, for example: physical skin location, age, and gender [21, 36, 40]. The thickest skin is found on the palm of the hands, the sole of the feet, and the back; while the thinest skin is found on the eyelid. The thickness of the subcutaneous tissue varies per person based on body mass and body fat. [21]

2.1.3 Color.

Skin color is primarily defined by the distribution of melanin and to a lesser extent by hemoglobin [27]. Melanin is a pigment found in two colors in the skin, brown-black or red-yellow [8]. Melanocytes cells, concentrated in the stratum basale layer of the epidermis, synthesize melanin in a complex process that ends with the transfer of melanosomes to keratinocytes, closer to skin surface [8, 21]. Hemoglobin is a protein found in red blood cells that transports oxygen through the body [5]. While skin color is primarily inherited, temporary changes in color are possible; for example, tanning from ultraviolet radiation exposure and reddening from inflammation [8].

2.1.4 Water and Skin.

Water is a vital part of healthy skin; it plasticizes keratin, consequently giving skin elasticity and preventing fractures [26, 34]. Furthermore, a poor hydration level is typically seen as a symptom of certain skin diseases [24]. Studies have been conducted to measure the water content found in the skin; in particular the stratum corneum, outermost layer of the dermis [26]. The final stage of keratinocytes after keratinization are known as corneocytes [21]. Experiments have shown that corneocytes swell as a function of hydration level at the stratum corneum layer [42]. Due to the enlargement of the cells, the thickness of the stratum corneum layer changes [9].

2.2 Spectroscopy

Spectroscopy is the study of the interaction between materials and electromagnetic radiation [10]. A photon is a discrete particle of radiation defined by a wavelength that corresponds to a energy level in the electromagnetic spectrum. Materials can absorb, reflect, or transmit photons. In the instance of a material that absorbs all incident radiation, known as a black body, materials can also emit photons. [4] The combination of interactions between a material and incident radiation, as a function of wavelength, results in a unique spectrum specific to the material's physical characteristic; this unique spectrum is known as a spectral signature [38].

2.2.1 Radiative Transfer Model.

In the absence of an atmosphere, radiation travels a path from the illumination source to the target and then finally to the sensor. The reflectance from the target becomes [25]:

$$\text{reflectance of the target} = \frac{\text{radiance at the sensor}}{\text{incident radiation at target}} \tag{2.1}$$

This spectrum is equivalent to the spectral signature of the target. Unfortunately, this is rarely achievable; in particular with remote sensing, where there is often a great distance between the illumination source, target, and sensor. The sensor-reaching radiation is influenced by multiple factors, some of which is shown in 2.2 [10].

2.2.2 Atmosphere and Illumination.

The atmosphere is rarely negligible, consequently, the measured reflection may be drastically different from the spectral signature of the target. Gases, aerosols, and molecules are present in the atmosphere, which absorbs and scatters radiation traveling between the illumination source and the target and again from the target to the sensor [38]. Absorption, apparent across the visible near infrared (VNIR) and SWIR regions, is mainly attributed to eight gases: water-vapor, carbon dioxide, ozone, nitrous oxide, carbon monoxide, methane, oxygen, and nitrogen dioxide [13]. Scattering, apparent in the lower visible (VIS) region, is mainly attributed to both aerosols and molecules [15].

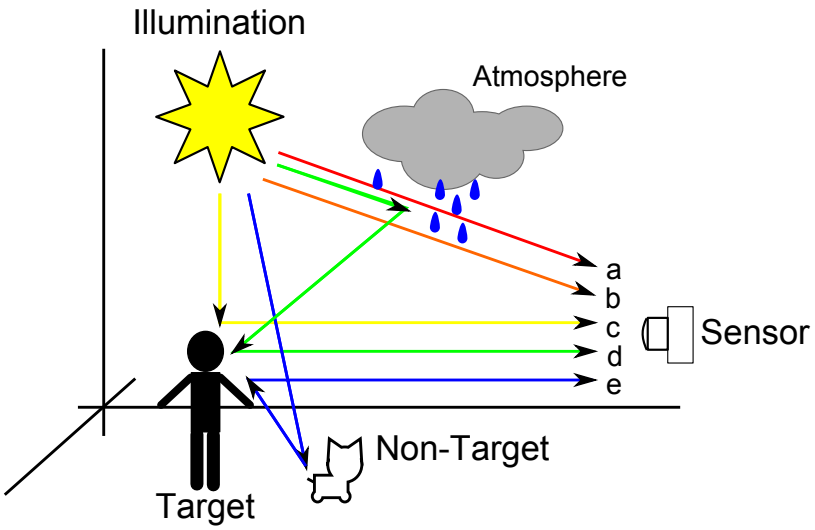

Figure 2.2: The sensor-reaching radiation could come from other sources, besides reflectance from the target. Five possible paths of travel are illustrated.

The Sun is used as an illumination source for ultraviolet, visible, and infrared radiation. While utilizing solar illumination, consider the time of day and season; factors that influences the angle of incident, intensity, and accessibility [39]. The sensor-reaching radiance of the Sun on a bright and cloudless day is seen in Figure 2.3. Absorption and scattering from the atmosphere is visible from the local minimums of the spectrum. Artificial illumination sources are also utilized, in place of the Sun. During data collects, the whole environment has to be carefully assessed to account for possible secondary illumination.

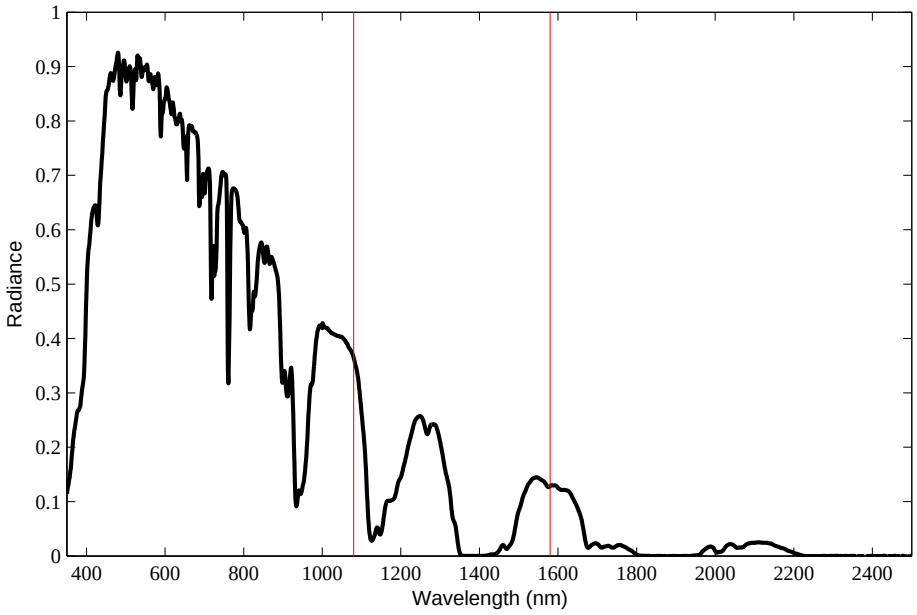

Figure 2.3: The sensor-reaching radiation of the Sun, measured from the ground on a bright and cloudless day. The local minimums demonstrates the influence of atmosphere from absorption and scattering. The two vertical red lines mark the two NDSI wavelength at 1080 nm and 1580 nm.

2.2.3 Water and Absorption Bands.

Water exhibits physical characteristics that have proven to be detrimental in radiometry. Of the eight absorbing gases mentioned in the previous section, water-vapor is the most prominent; affecting about half of the VNIR and short-wavelength infrared (SWIR) region [13]. At various widths and strength, water-vapor absorption bands exists at: 600 nm, 660 nm, 730 nm, 820 nm, 910 nm, 940 nm, 1140 nm, 1375 nm, 1900 nm, and 2500 nm, in ascending order of strength [13, 15]. Water-liquid absorption bands exists at approximately: 1500 nm, 1950 nm, and 2500 nm [22]. A plot of the absorption coefficient for water-liquid is shown in Figure 2.4. Besides location on the electromagnetic spectrum, absorption strength is also dependent on the abundance of water [18, 19].

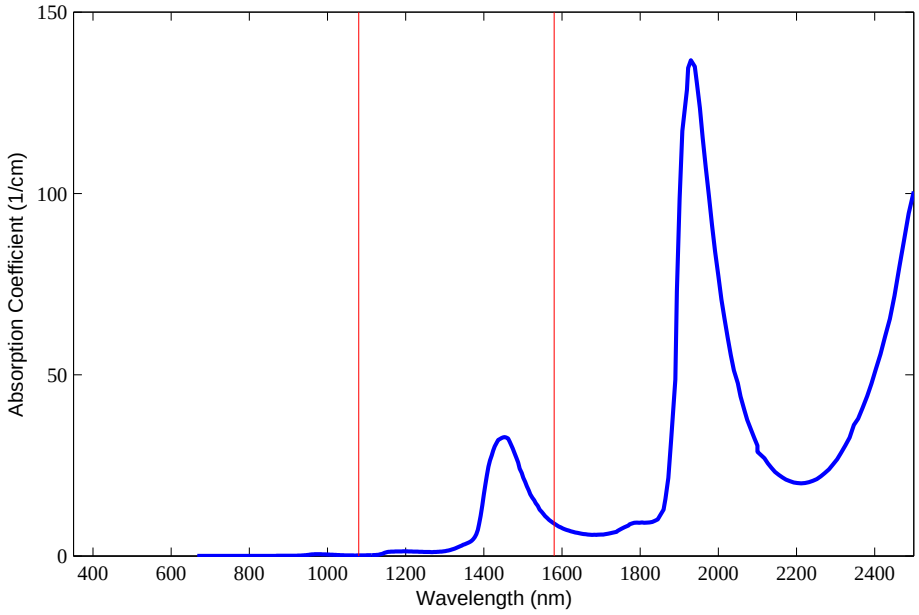

Figure 2.4: Absorption spectrum of liquid and ice water. Major water absorption bands exist at 1500 nm, 1900 nm, and 2500 nm. [22] The two vertical red lines mark the two NDSI wavelength at 1080 nm and 1580 nm. Water absorption may pose a problem to the latter NDSI wavelength.

2.3 Spectral Signature of Skin

An example of skin spectral signature is shown in Figure 2.5. While skin is a complex multilayer structure that features numerous components, a reasonable spectral model can be developed by three parameters: water, hemoglobin, and melanin, due to their strong absorption [35]. An overlay of the three parameter's absorption coefficient is shown in Figure 2.6. In the VIS region, skin spectrum is predominately affected by melanin and hemoglobin; water absoprtion is mostly observed at higher wavelengths. As discussed in Section 2.1, skin may vary considerably per person. A plot of skin spectra from two different subjects described as light and dark-brown on the Fitzpatrick scale is shown in Figure 2.7 [27]. The most apparent difference between the subjects is melanin abundance; as expected, reflectance is lower for the dark-brown subject in the VIS region.

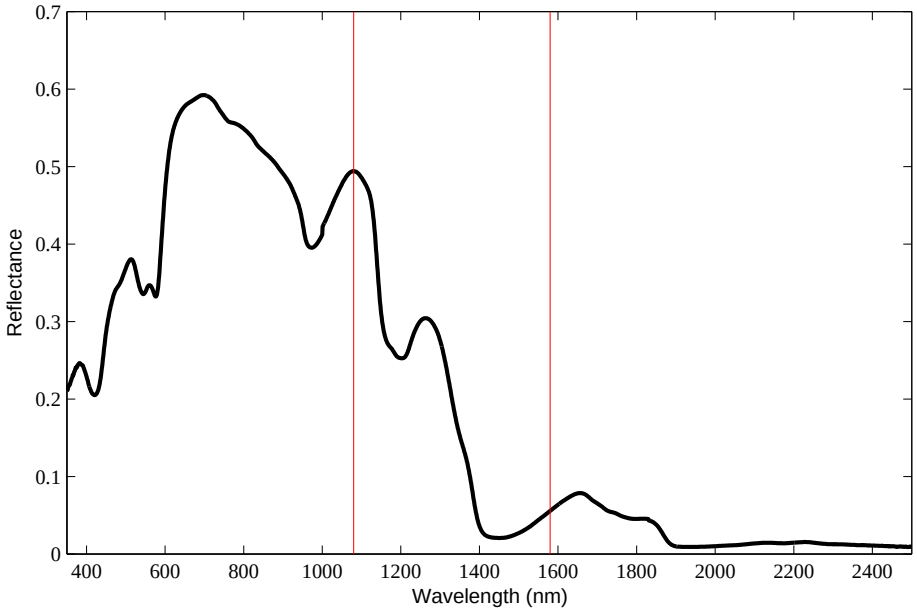

Figure 2.5: Spectral signature of human skin. The two vertical red lines mark the two NDSI wavelength at 1080 nm and 1580 nm. The wavelengths were chosen to correspond to a local maximum and a local minimum [35].

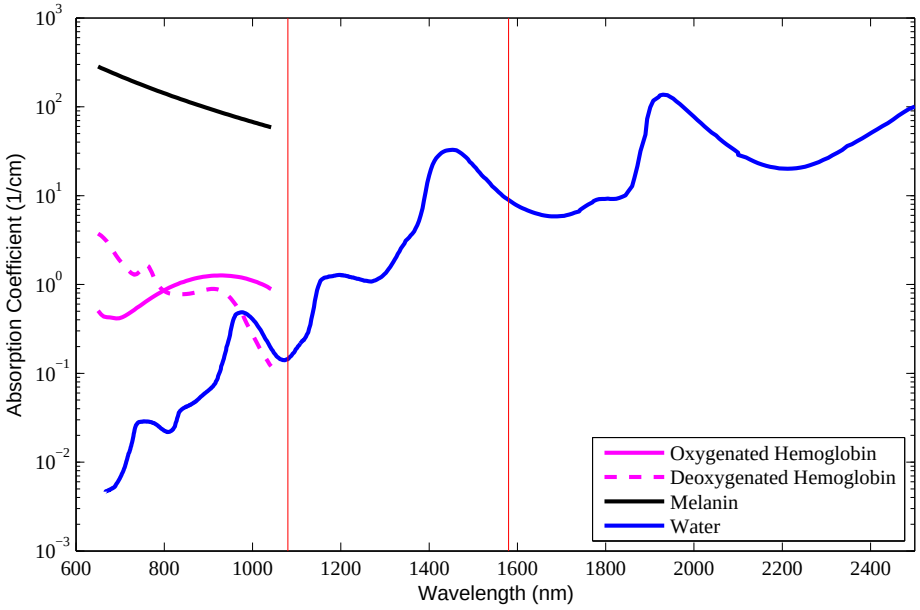

Figure 2.6: The absorption coefficient of water (blue), hemoglobin (pink), and melanin (black), the major components used to model skin [16]. The two vertical red lines mark the two NDSI wavelength at 1080 nm and 1580 nm.

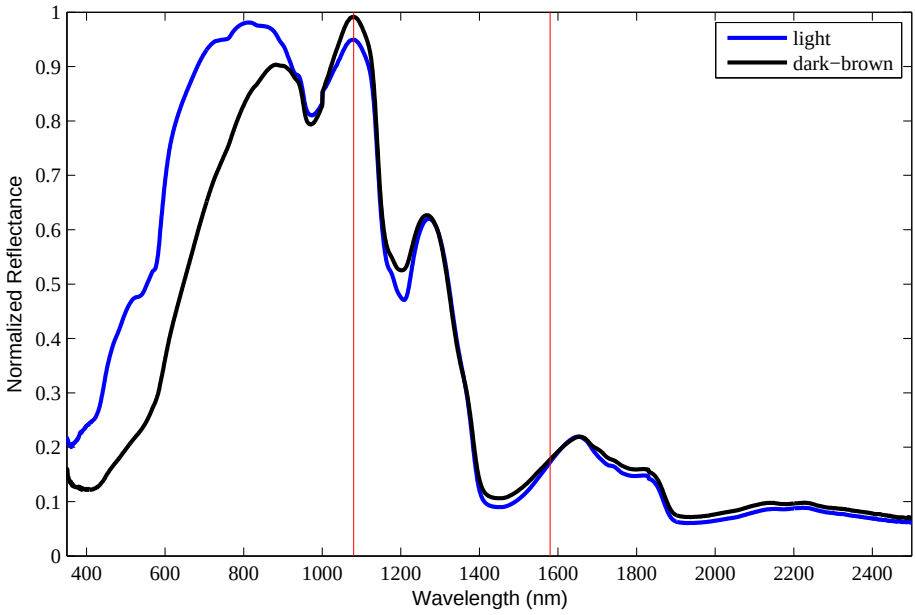

Figure 2.7: The spectral reflectance of skin for two skin colors, light (blue line) and dark-brown (black line). Darker skin has more melinan, which is apparent in the plot from the lower reflectance in the visible region. The two vertical red lines mark the two NDSI wavelength at 1080 nm and 1580 nm.

2.4 NDSI

The Normalized Difference Skin Index (NDSI) function is defined by two different wavelengths in the NIR and SWIR regions of the electromagnetic spectrum such that:

$$\text{NDSI} = \frac{\lambda(1080) - \lambda(1580)}{\lambda(1080) + \lambda(1580)} \tag{2.2}$$

where $\lambda(1080)$ and $\lambda(1580)$ are the reflection of the target at 1080 nm and 1580 nm respectively and $-1 < \text{NDSI} < 1$ [35]. An examination of skin spectrum shows that 1080 nm corresponds to a local maximum and 1580 nm corresponds to a local minimum. These two points were chosen in creation of NDSI to mimic the Normalized Difference Vegetation Index (NDVI) [35]:

$$\text{NDVI} = \frac{\lambda(860) - \lambda(670)}{\lambda(860) + \lambda(670)}. \tag{2.3}$$

NDVI is commonly used in the field of remote sensing for vegetation. The index utilizes two wavelengths, one in the VIS region and the other in the NIR. The first, 670 nm, corresponds to a minimum caused by chlorophyll absorption. The second, 860 nm, corresponds to a maximum caused by vegetation canopies reflection. [12]

NDSI is commonly used in combination with another index, the Normalized Difference Green Red Index (NDGRI) [35]:

$$\text{NDGRI} = \frac{\lambda(540) - \lambda(660)}{\lambda(540) + \lambda(660)}. \tag{2.4}$$

The index utilizes two wavelengths in the VIS region; 540 nm corresponds to the color green and 660 nm corresponds to the color red. Vegetation and water-bearing objects with high scatter tend to have NDSI values similar to human skin, potentially causing false positives in certain environments. However, since human skin is more red than green, NDGRI is applied in those environments to suppress false detections. NDVI can also be used in place of NDGRI; each index has their advantages in different situations. [35]

Thresholding is the basic premise of NDSI for spectral skin detection. Given a spectral image, there are three steps in this detection method. In the first step, NDSI is computed for all of the pixels in the spectral image to generate a grayscale image from -1 to 1. Next, either NDVI or NDGRI is used to generate another grayscale image from -1 to 1. Finally, from these two grayscale images, a binary image is generated based on the following rule [35]:

$$S_i = \begin{cases} 1 & \text{if } a_1 \le a_i \le a_2 \text{ and } b_1 \le b_i \le b_2 \\ 0 & \text{otherwise} \end{cases} \tag{2.5}$$

where $S_i = 1$ when the *ith* pixel is classified as skin or $S_i = 0$ otherwise. The variables a_1 and a_2 are the lower and upper threshold for the computed NDSI a_i, while b_1 and b_2 are the lower and upper threshold for the computed NDVI/NDGRI b_i for skin. The resulting binary image should highlight all of the skin pixels in the original spectral image. Determining the thresholds is the challenge of this skin detection method.

2.5 Chapter Summary

Four important topics were covered in this chapter that is essential to understanding this thesis. First, the anatomy and physiology of human skin was addressed. Second, spectroscopy and the factors/considerations in spectral analysis were covered. Third, the spectral signature of skin was presented with a short rational for its spectrum. Lastly, how NDSI was derived and used was discussed.

III. Methodology

3.1 Data Acquisition System

Reflectance measurements are collected using a FieldSpec® 3, a field portable spectroradiometer manufactured by Analytical Spectral Devices (ASD), shown in Figure 3.1; henceforward referred to as the FieldSpec or the spectroradiometer. What separates a spectroradiometer from a general spectrometer is it's ability to take measurements in radiance and irradiance. After calibration and with proper software implementation, the FieldSpec can also be used for reflectance and transmittance measurements. [28]

Figure 3.1: The ASD FieldSpec® 3 spectroradiometer attached to the ASD contact probe. The computer is for the software that controls the FieldSpec.

3.1.1 Operations [28].

The FieldSpec operates in the visible through short-wavelength infrared (SWIR) regions of the electromagnetic spectrum with the use of three detectors. The visible near infrared (VNIR) detector features a 512-channel silicon photodiode array for wavelengths of 350 nm to 1000 nm. The SWIR region is separated in two subregions, SWIR1 and SWIR2, featuring a scanning concave grating system and a Indium Gallium Arsenide detector. SWIR1 covers the wavelengths of 1000 nm to 1830 nm while SWIR2 covers 1830 nm up to 2500 nm. The detectors converts the incoming photons into voltage which is then processed with a 16-bit analog-to-digital converter to generate the displayed signal. The VNIR and SWIR sensors have a sampling interval of approximately 1.4 nm and 2 nm respectively, wavelength depended.

3.1.2 Field-Of-View.

The field-of-view of the spectroradiometer is primarily defined by two parameters, the angular field-of-view of the optic lens and the distance from the optic lens to the target [28]. The FieldSpec collects electromagnetic radiation through a fixed fiber optic cable with a 25° field-of-vision. The cable is housed in two ASD accessories, the pistol grip and contact probe, in order to control the field-of-view during the experiments. For near field measurements, 1 meter or less, the diameter of the field-of-view is defined as [28]:

$$Y = D + 2 * X * tan(A/2) \tag{3.1}$$

where Y is the diameter of the field-of-view, D is the effective diameter of the foreoptic lens, X is the distance to the target, and A is the foreoptic angular field-of-view. A diagram of the parameters can be seen in Figure 3.2.

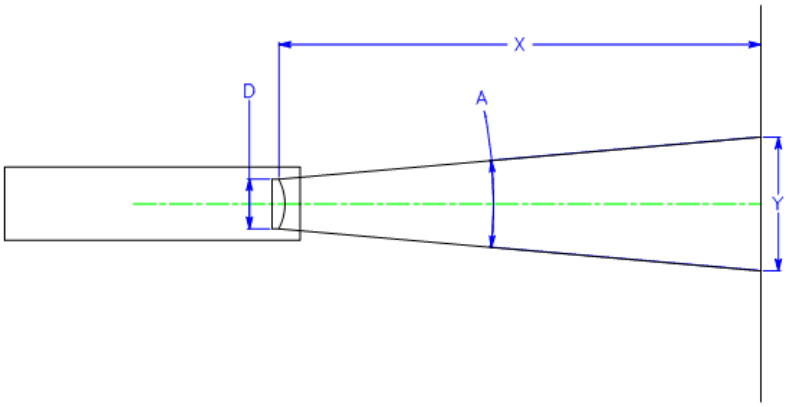

Figure 3.2: Parameters that define the FieldSpec's field-of-view: Y is the diameter of the field-of-view, D is the effective diameter of the foreoptic lens, X is the distance to the target, and A is the foreoptic angular field-of-view [28].

To verify the field-of-view, an additional procedure is performed at the start of the every data collect. Black markers, chosen for its absorptive properties, are placed on the boundary of the field-of-view to outline the area. This boundary is determined by sliding four black markers in and out of the view-of-field at four equal-distance points. The FieldSpec displays a real-time measurement of the field-of-view. Once inside the area, a sudden drop in reflectance is apparent on the spectral display; similarly, once outside the area, the displayed spectrum returns to before. These marks become necessary for computations, discussed later.

3.1.3 Calibration.

The FieldSpec collects radiance measurements in its default mode of operation. In order to collect data in terms of reflectance, the spectroradiometer has to be calibrated beforehand. The ASD application software used to control the spectroradiometer, RS^3, has a built in function for reflectance calibration given a white reference standard. Again, reflectance is the ratio of sensor reaching radiance to the incident radiation [25]. Targets made from materials that reflect near 100%, white reference panels, provides us a known

reflectance spectrum. Three Spectralon® white reference panels manufactured by Labsphere are utilized in the experiments, shown in Figure 3.3. These reference panels have been designed to reflect 95% to 99% across the range of the spectroradiometer, 350 nm to 2500 nm [28]. In combination with an invariant illumination source, a baseline is determined for the spectroradiometer; resulting in reflectance measurements.

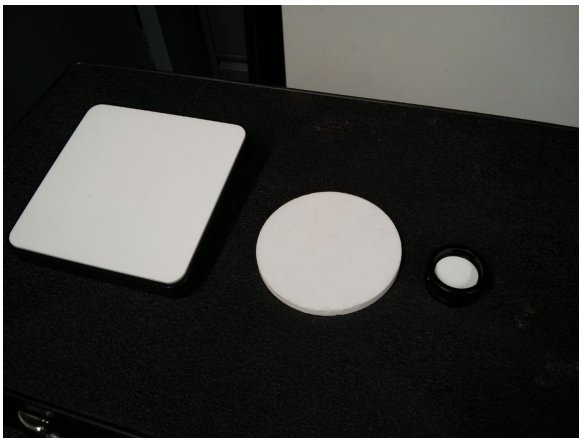

Figure 3.3: An image of the three white reference panels used in the experiments.

In the absences of any electromagnetic radiation, a signal can still be measured by the FieldSpec. This intrinsic signal of imaging systems, known as dark current, is generated from random internal electrons detected by the sensors. Since dark current is relatively constant, the system is calibrated by a simple subtraction of the average dark current [28]. RS^3 has a built in function for dark current subtraction.

The spectroradiometer has to be optimized to the illumination source, prior to calibration. At start up, with the white reference panel and illumination source in place, the FieldSpec is set up to display the radiance of the source. For correct measurements, the illumination source must radiate across the electromagnetic range of the spectroradiometer, 350 nm to 2500 nm. A valid spectrum for an illumination source is shown in Figure 3.4(a). If the spectroradiometer is oversaturated by the source,

optimization scales the readings of the sensors. On the other hand, if the spectroradiometer is under saturated and optimization does not address the issue, a higher power source is needed. RS^3 has a built in function for optimization.

After optimization and calibration, the FieldSpec will display a constant signal of one with a white reflectance panel, as shown in Figure 3.4(b). Calibration should be performed periodically during the data collects; slight variations, such as a change in the illumination, can cause an off-set in the data. To check on the calibration, the white reference panel is used in between measurements. If the reflectance of the panel deviates from the constant line of one, recalibration is necessary.

Non-solar illumination sources require time to reach a steady state of electromagnetic output. Known as warm up times, these lamps do not achieve their full output right at start up. To avoid problems that may arise from a varying illumination source, wait at least 10-15 minutes before use.

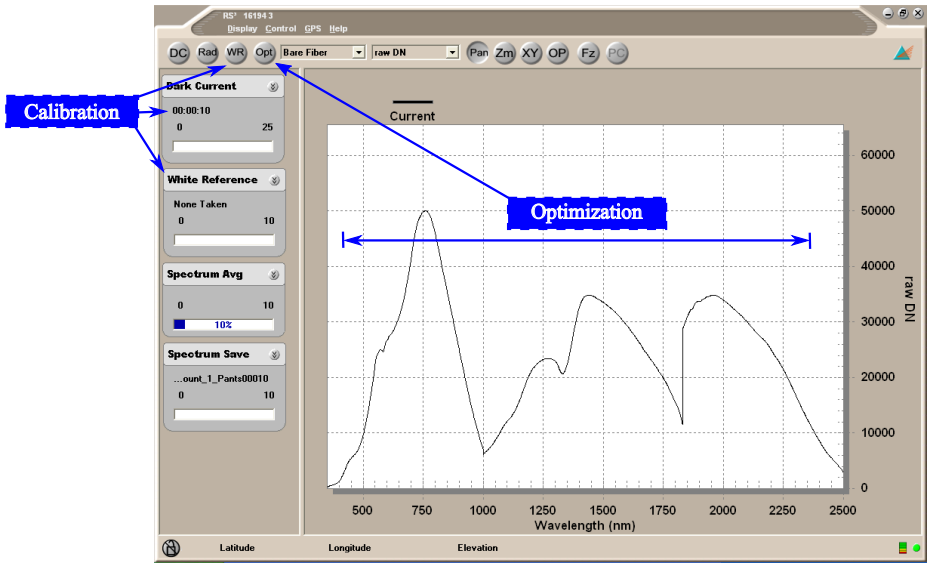

(a)

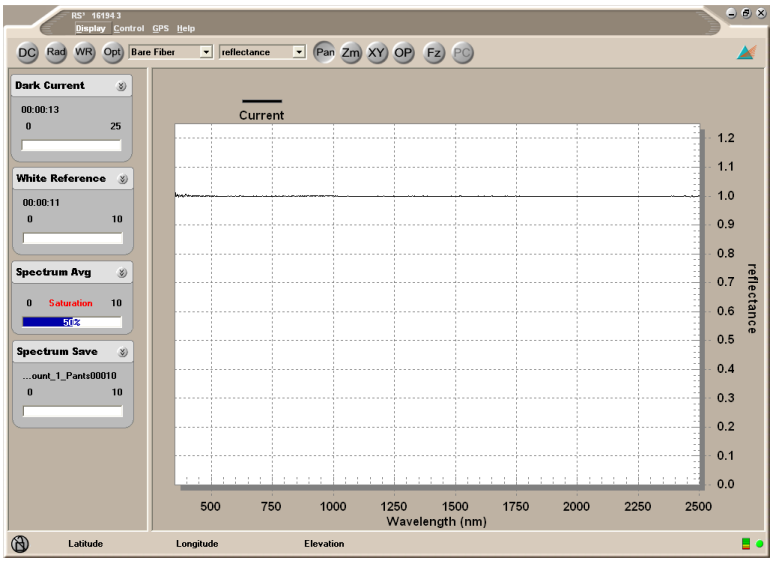

(b)

Figure 3.4: Screenshots of RS^3, the ASD software used to operator the FieldSpec. On start up, the ASD has to be optimized and calibrated for reflectance measurements and dark current subtraction; (a) The display after proper optimization, there should be a reading for across the whole spectrum of 350 nm to 2500 nm; (b) The display after dark current subtraction and white reflectance.

3.2 Experiment Configurations

Two different configurations with the FieldSpec are utilized to conduct the experiments. The field-of-view requirement for the experiments dictates configuration selection. For mixed pixel experiments, the field-of-view has to be precisely defined for skin percentage. The general equipment set up for the mixed pixel configuration is shown in Figure 3.5. The optics cable is housed in the pistol grip above the target area and pointed downwards; in this orientation, undesired radiation, not reflected from the target, is minimized from the narrow opening of the pistol grip. Two external halogen lamps, ASD Pro Lamps, are used as the illumination source; these broadband lights, with tungsten-halogen bulbs, radiates from 350 nm to 2500 nm, covering the required electromagnetic range. The target, shown in Figure 3.6, depicts the top-down field-of-view of the spectroradiometer. The distance to the target, X, is defined from tip of the pistol grip to the top plane of the rectangular solid that represents the target in Figure 3.6. The background of the pixel spans the inside of the rectangular solid.

The other configuration is used to obtain spectral signatures; in this set up, the optics cable is used in conjunction with the ASD contact probe, shown in Figure 3.1. The contact probe features a built in illumination source, halogen bulb, that covers the required electromagnetic range of 350 nm to 2500 nm. In operation, the contact probe is lightly pressed into the target, creating a seal from the atmosphere. At this point-blank range, measurements using the contact probe can be considered free of interference from the atmosphere and undesired radiation.

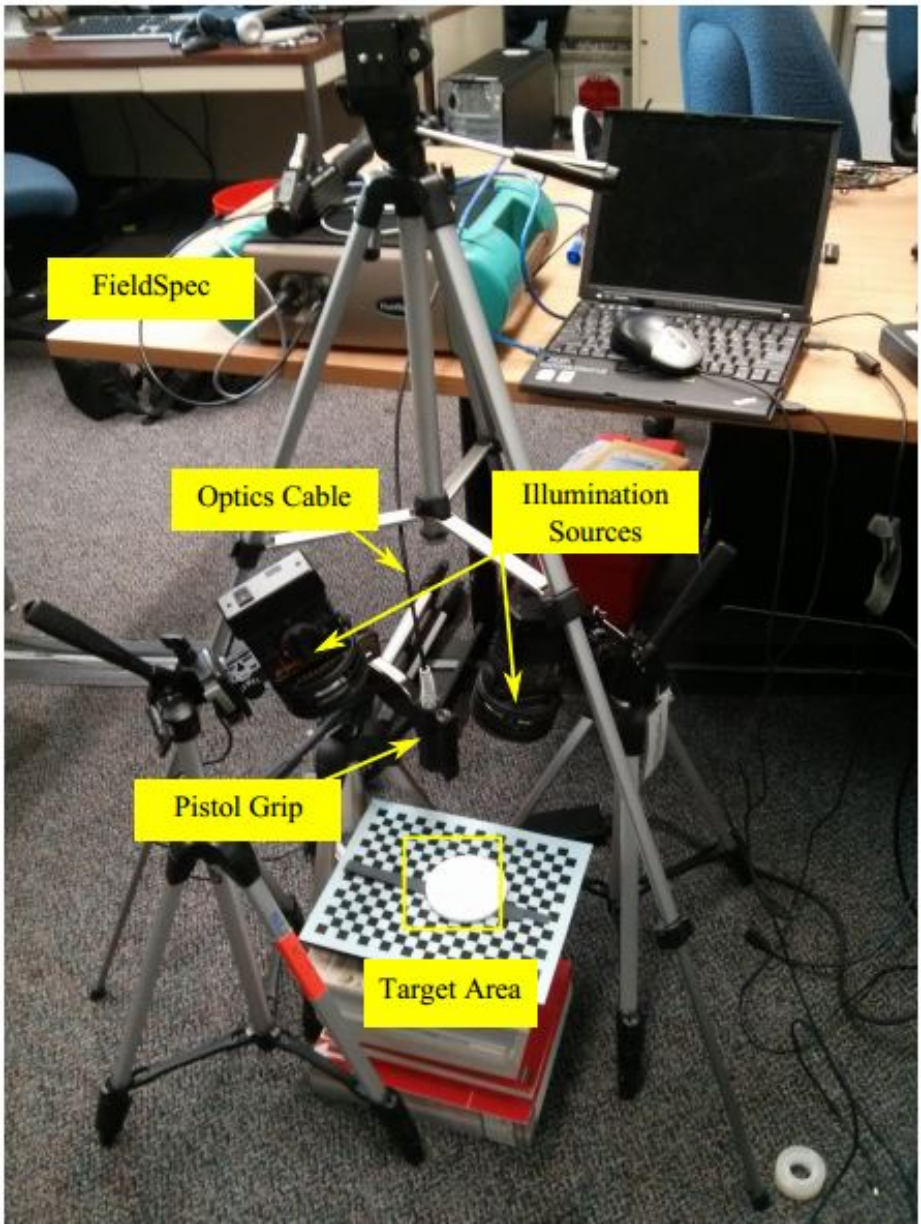

Figure 3.5: The mixed pixel configuration. The major equipment used in this configuration and the target area are highlighted in yellow.

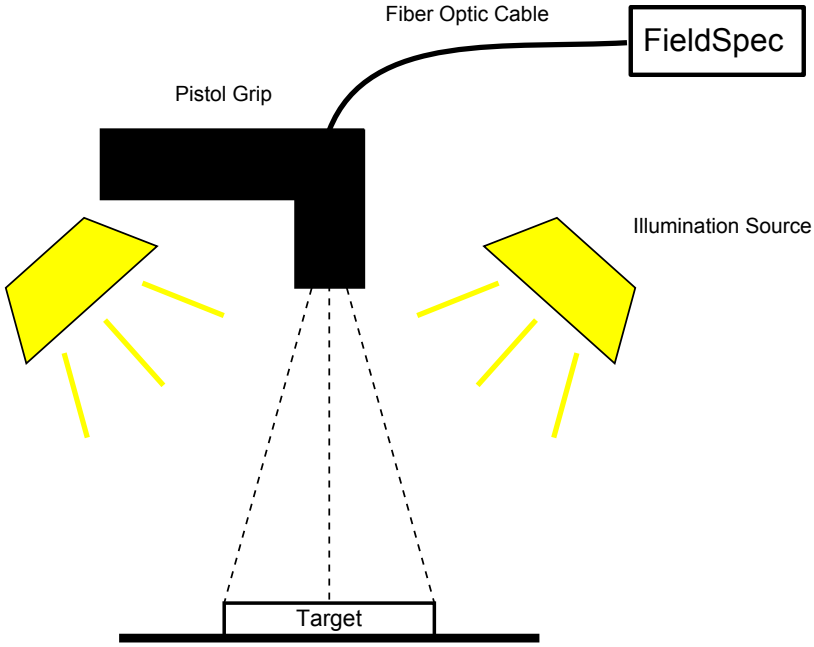

(a)

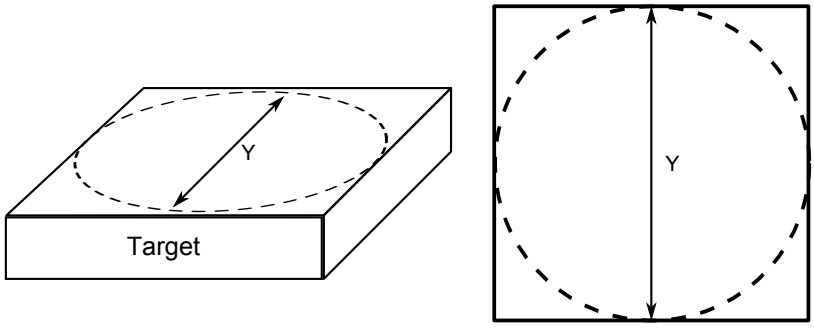

(b)

Figure 3.6: The configuration for mixed pixel experiments featuring the pistol grip and the two illumination lamps; (a) Side view of the set up; (b) Side and top-down view of the target area where Y is the diameter of the field-of-view.

3.3 Water

The Environmental Protection Agency of the United States has nine categories of water, e.g. drinking, ground, oceans, and wetlands [31]. Water is mainly categorized by the chemicals, microscopic organisms, and physical particles they contain. For example, fluoride is commonly added to drinking water, as recommended by the World Health Organization [32]. Remote sensing of shallow coastal waters reveals other materials in addition to water e.g. sand, algae, macrophyte [23]. These chemicals, microscopic organisms, and physical particles have their own spectral properties; all of which influences the measured spectrum of the water. Distilled water is water in its pure form, free of any additional elements. In this thesis, distilled water is used in the experiments.

3.4 Skin Percentage Extraction

For certain mixed pixel experiments, the skin percentage in the pixel has to be computed. With the methodology utilized in this thesis, skin percentage has to be computed after data acquisition. Specifically, skin percentage is defined as the area of skin to the area of the field-of-view To obtain these areas, an optical camera is suspended above the spectroradiometer, providing a top-down view of the target area. For each sample taken by the FieldSpec, an image of the mixed pixel is captured by the camera.

ImageJ is an image processing software that features a capability to take area measurements. First, the field-of-view is extracted using the circular selection tool and with the assistance of black markers placed in the image. Next, the extracted area is measured and a mask is created to mark off the view-of-field in the other images, without the black markers. For each of the following images, the skin within the view-of-field mask is extracted using the manual selection tool. The extracted area is measured and then divided by the field-of-view area to compute the skin percentage for the sample associated with the image. An overview of the skin percentage extraction process with ImageJ is shown in Figure 3.7.

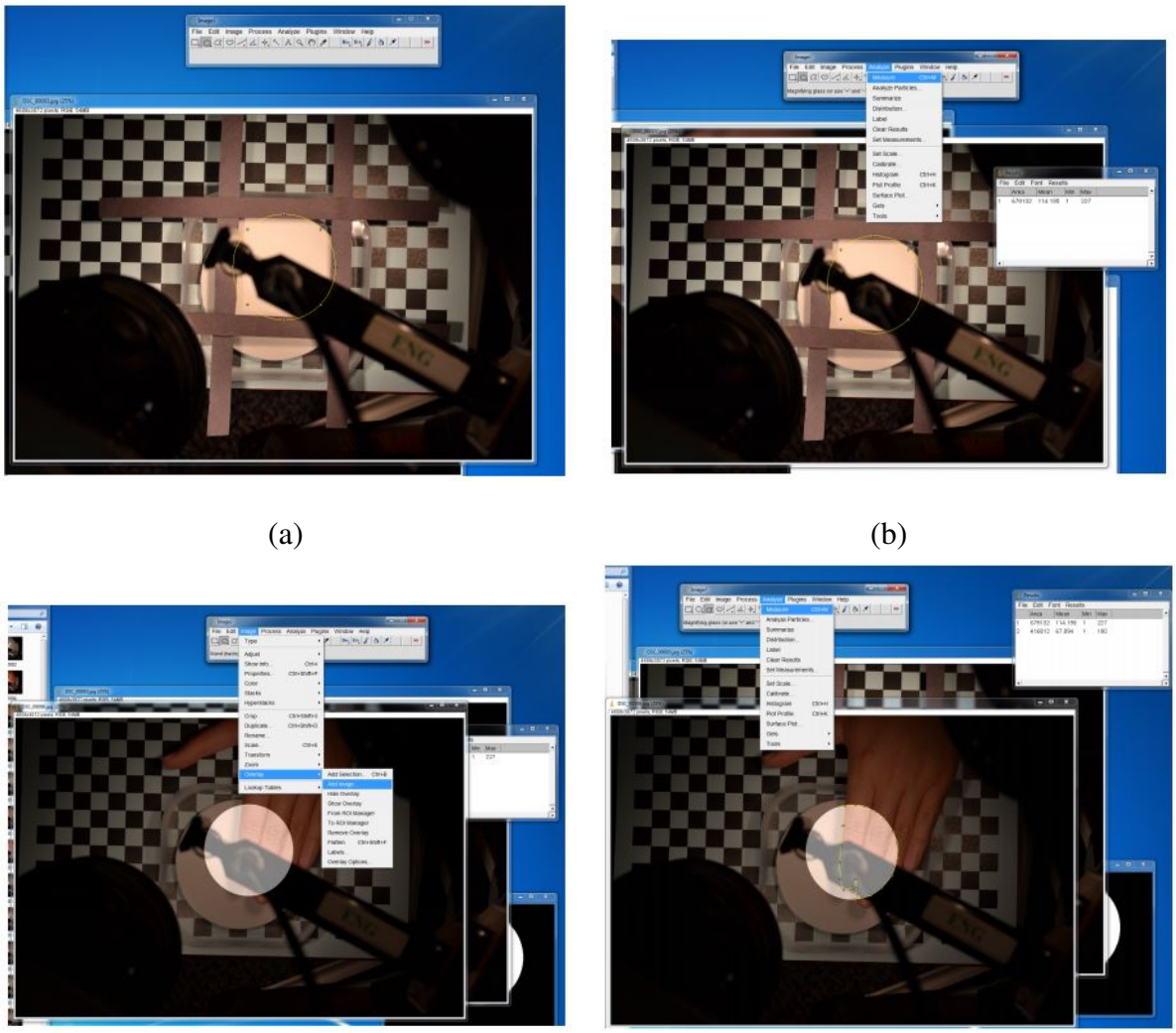

(a) (b)

(c) (d)

Figure 3.7: Screenshots of the skin percentage extraction process using ImageJ, a image processing software; (a) The black markers define the boundary of the field-of-view. A circular selection tool is used to select the area; (b) Measurement of the selected field-of-view circle; (c) An image of a mixed pixel with the field-of-view mask applied; (b) A manual selection tool is used to select the skin in the field-of-mask for measurement.

3.5 Data Processing

The data collected from the FieldSpec is saved under an ASD proprietary file format. ViewSpec Pro, an ASD post-processing software, is used to import the collected data into an ASCII, comma-separated value format for further analysis. MATLAB®, a numeric computational software, is used to calculate the Normalized Difference Skin Index (NDSI) for the collected data using Equation 2.2. In spectral analysis of two or more spectra, the reflectance spectrum for the samples are first normalized by dividing by highest value of that sample. When applicable, a linear trend line is fitted to the NDSI plots using MATLAB's Figure Basic Fitting tool.

3.6 Chapter Summary

This chapter details the equipment, software, procedures, and highlighted a few considerations for calibration and normalization that should implemented during the experiments.

IV. Results

4.1 Experiment 1 - Water Background

The objective of the first experiment is to answer the question: How does a mixed pixel of skin with water in the background impact Normalized Difference Skin Index (NDSI)? While a person may be in or exposed to a body of water, there is a possibility that some aspect of their skin remains dry. From the perspective of a sensor, water appears relatively next to the person, in the background. In this instance, mixed pixels of skin and water forms, particularly around the outline of the person. To determine how NDSI is impacted, a data set is collected and assessed.

4.1.1 Data Collection.

In this experiment, a data set of reflectance spectra is created from mixed pixels of skin with water in the background. The water in the background is held constant, while the amount of skin in the pixel varies. The experiment is set up according to the mixed pixel configuration, shown in in Figure 3.5. The tip of the pistol grip measures a distance of 12.7 cm from the top plane of the target. No foreoptics are used with the pistol grip, leaving the angular field-of-view of the bare optics cable of 25°. Using Equation 3.1 with a substitution of $A = 25$ and $X = 12.7$ cm yields the field-of-view:

$$Y = 0 + 2 * 12.7cm * tan(25/2) = 5.63cm \tag{4.1}$$

A plastic container for the water background is placed on the target area platform. To prevent interferences from the container and platform, such as light transmission through the clear plastic to the platform and reflection back, a white reference panel is placed at the bottom of the container for complete reflectance. The container is filled with approximately 3 mm to 4 mm of distilled water, measuring from the top of the white reference panel. For human skin, the back of a subject's hand is used, shown in

Figure 4.1(a). Prior to each data collect, the skin sample area is washed with soap and water.

Samples are taken as the subject moves their hand, palm down, across the field-of-view at a slow rate; at specific skin percentages, data is collected. Each sample consists of a reflectance measurement from the FieldSpec and an image from the optical camera, for skin percentage extraction. A histogram of the samples are shown in Figure 4.2, illustrating a spread of samples across the skin percentages.

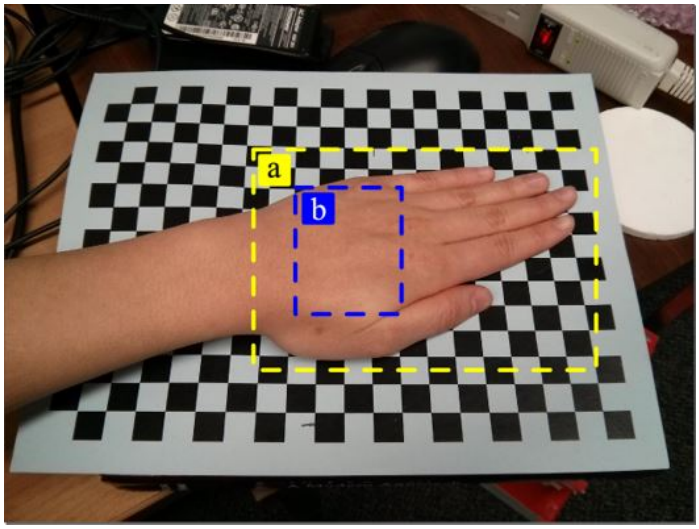

Figure 4.1: An image highlighting the two areas human skin samples were collected from in the experiments. For Experiment 1 and 3, area (a) was used. For Experiment 2 and 4, area (b) was used.

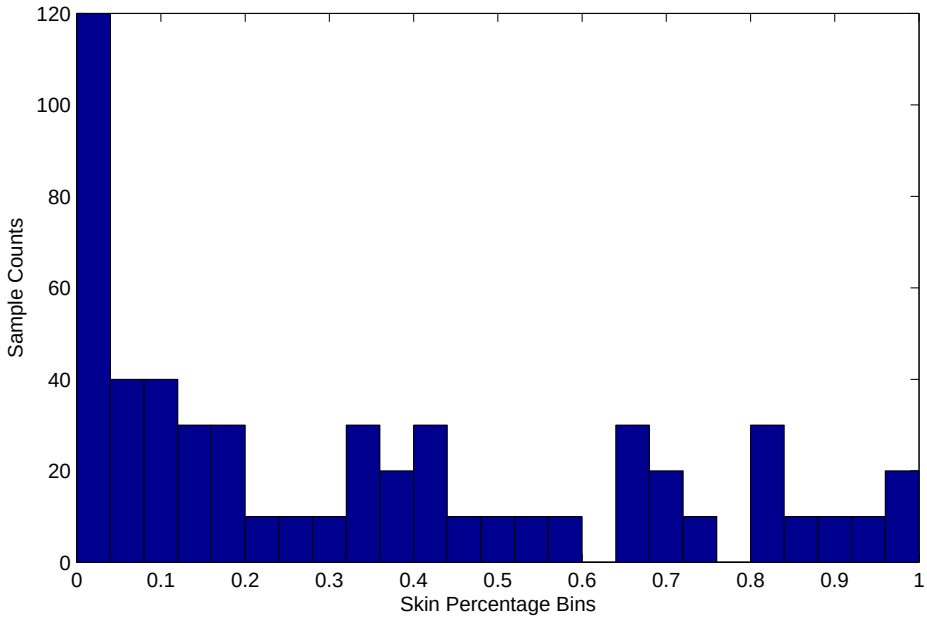

Figure 4.2: Histogram of the data set from Experiment 1 (Water Background). An even distribution of data is collected of various skin percentages.

4.1.2 NDSI Evaluation.

The resulting NDSI values for the data set collected in Experiment 1 are shown in Figure 4.3 as a plot of the skin percentage versus the NDSI, with error bars denoting the standard deviation and a fitted linear line for reference. For a mixed pixel of 100% skin and 0% water, NDSI is approximately 0.7. Using the thresholding method for skin detection from Equation 2.5, a_1 and a_2, the lower and upper NDSI threshold respectively, should be ideally set to a small range around 0.7084. But, there is a trade-off between the

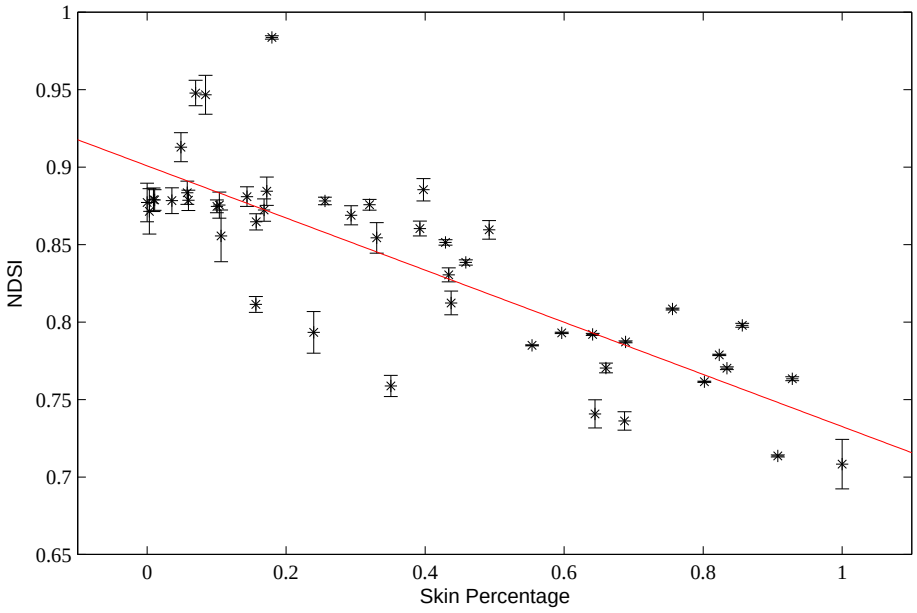

Figure 4.3: NDSIs of the data set from Experiment 1 (Water Background). The error bars denotes the standard deviation. The red line is a linear fitted line for reference. There is a wide spread in the range of NDSI values for skin-positive mixed pixels. A 100% skin pixel has a NDSI of approximately 0.7, while a 10% skin pixel has a NDSI of appropriately 0.85.

threshold range and the probability of detection versus false detection. For a mixed pixel of skin with water in the background, NDSI is varied from approximately 0.7 to 1.0 as a function of skin percentage. For a mixed pixel of 10% skin and 90% water, NDSI is

approximately 0.85. To detect that skin pixel, the upper NDSI threshold has to be increased greatly, hence increasing the probability of false detection. In the case of the bright and cloudless day, Nunez reported a NDSI threshold range of 0.65703 to 0.76779 [35]. Based on those thresholds, the detector is only capable of classifying mixed pixels with at least 64% skin or more.

There is a wide range in NDSI values because of the nonlinear relationship between the two parameters of the NDSI function and the nonlinear mixing between skin and water background. To demonstration the nonlinearity, given the average reflectance spectrum of 100% skin-0% water, $\lambda(1080) = 0.6077$ and $\lambda(1580) = 0.1039$:

$$NDSI_{100\%skin-0\%water} = \frac{0.6077 - 0.1039}{0.6077 + 0.1039} = 0.7080 \tag{4.2}$$

Suppose 60% water is introduced to the pixel and the reflectance at 1580 nm lowers to $\lambda(1580) = 0.0469$. For NDSI to hold constant at 0.7090 in this example, $\lambda(1080)$ has to be:

$$\lambda(1080) = \frac{\lambda(1580)(1 + NDSI)}{(1 - NDSI)}, \tag{4.3}$$

as derived from the NDSI function. Substituting the values from before yields:

$$\lambda(1080) = \frac{0.0469(1 + 0.7090)}{(1 - 0.7090)} = 0.2754. \tag{4.4}$$

But, $\lambda(1080) = 0.2754$ is not true, instead, $\lambda(1080)$ measured to be 0.5473. From the resulting NDSI values, it is apparent the relationship between the two NDSI parameter is not held constant with the varying skin percentage and water background.

Furthermore, the mixed pixel does not follow a linear mixing model. In a linear mixing model, the measured spectrum of a mixed pixel represents an average of the material in the pixel as a function of each material's abundance. Figure 4.4 shows four reflectance spectra: 100%skin-0%water, 0%skin-100%water, 50%skin-50%water, and the theoretical spectrum for a linear mixing model at 50%skin-50%water. The linear mixing model is derived from the average of the 100% skin and 100% water samples. There is little

resemblance between the measured spectrum and the linear model. To see the spectra for the other skin percentage verse their theoretical linear mixing model, refer to Appendix A.

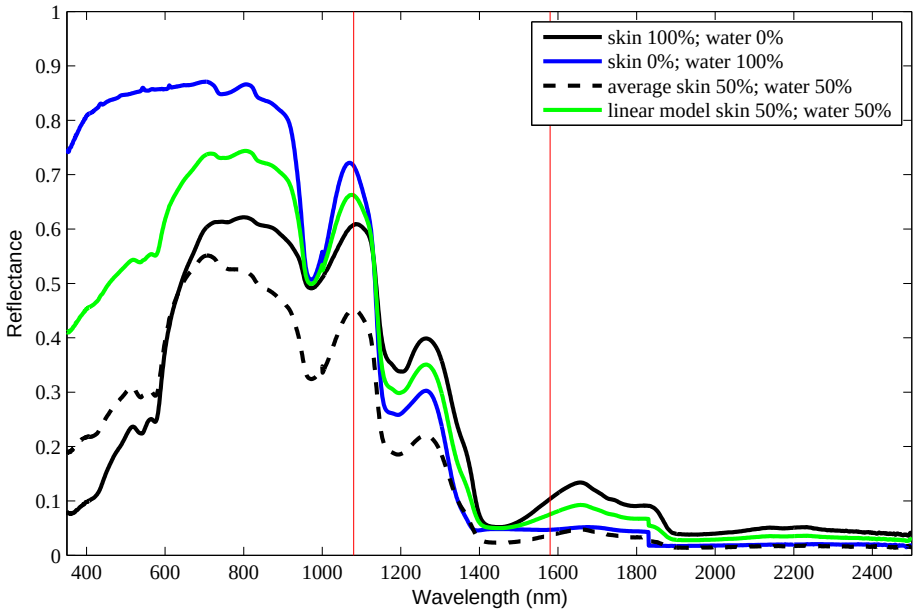

Figure 4.4: The spectral reflectance of a mixed pixel of skin with water in the background at %100 skin (black), 0% skin (blue), 50% skin (green), and the theoretical linear mixing model of 50% skin (dashed). The mixed pixels from Experiment 1 does not fit a linear mixing model, or else the green and dashed lines would overlap.

A possible explanation for this result is the complex distribution of materials in the pixel; skin is measured from a horizontal plane approximately 3 cm above the water. The distance between the skin and water can cause multiple issues. For example, since the illumination lamps are placed at an angle, radiation could travel between the skin and water before reaching the sensor, multiple path radiation. Also due to the angle of the illumination lamps, shadows could be cast from the skin onto the water, blocking radiation. An image captured by the optic displaying these shadows is shown in Figure 4.5. In addition to the distribution issue, the spectral reflectance of the hand could also be another problem. There are spectral variations between the lower back of the hand, the fingers, and the fingernails, but all of which are categorized as the same material, skin. The linear mixing model is developed from a sample collected from the lower back of the hand; creating a generalization that may be inaccurate for some samples.

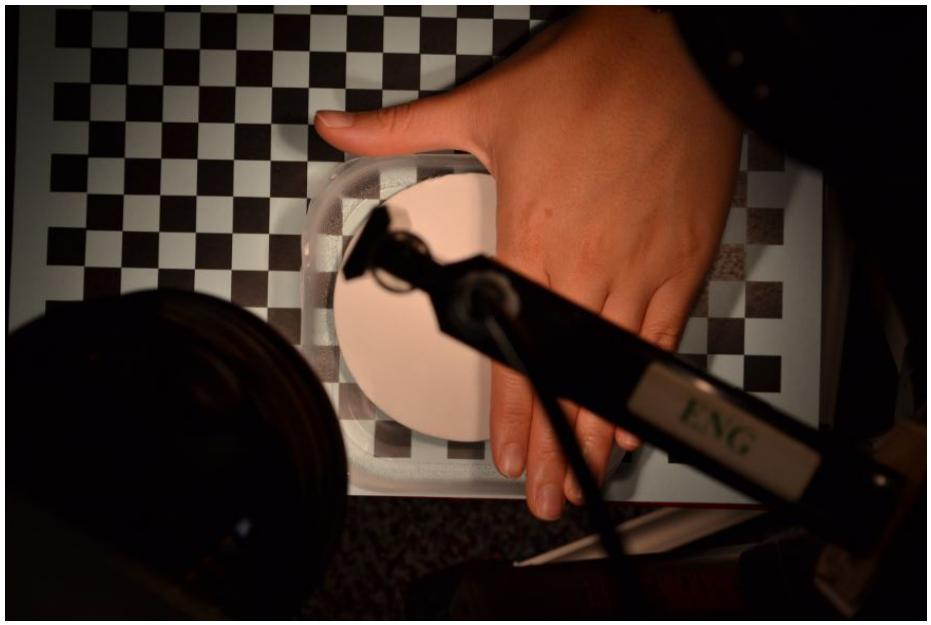

Figure 4.5: An image captured in Experiment 1 from the optical camera suspended above the set up configuration. Shadows are casted by the hand due to the angle of the illumination source. These shadows influences the measured reflectance spectrum.

Other materials are also used as the background: cloth, sand, and grass, to evaluate whether the results of this experiment are unique to just backgrounds of water. To see the collected data set, refer to Appendix B, C, D. The resulting NDSI values for these experiments are shown in Figure 4.6. From an visual inspection, an apparent difference between water versus the other backgrounds is the decrease of NDSI as skin percentage increase. With the other background materials, the NDSI increases as skin percentage increase. Again, this result stems from the physical characteristic of water; water exhibits strong absorptive properties in the short-wavelength region unlike: cloth, sand, and grass. Using Nunez's threshold of 0.65703 to 0.76779 for comparison between the background materials: cloth requires 78%+, sand requires 72%+, and grass requires 70%+ in a mixed pixel with skin for detection, while water requires 64%+. Of the four evaluated background materials, NDSI is the most robust with water.

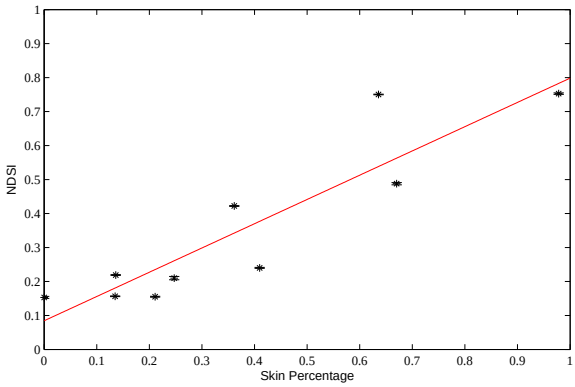

(a)

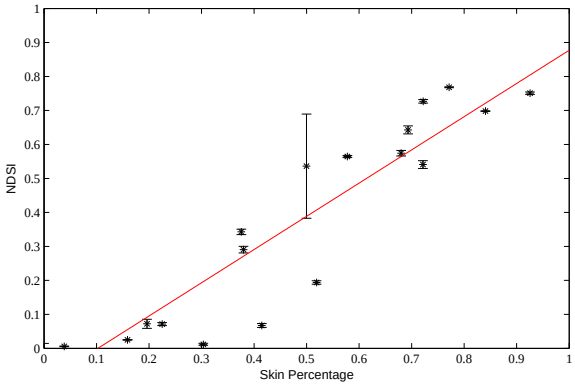

(b)

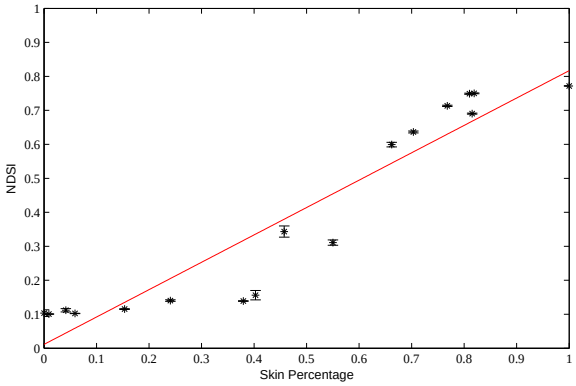

(c)

Figure 4.6: The NDSIs of the data set from Experiment 1 using other background materials: (a) cloth, (b) sand, and (c) grass. The error bars denotes the standard deviation. The red line is a linear fitted linear for reference. NDSI values increases as skin percentage increase, unlike the water background.

4.2 Experiment 2 - Water Droplets

The objective of the second experiment is to answer the question: How does a mixed pixel of skin with water droplets on surface of the skin impact NDSI? After skin is submerged and removed from body of water, some form of the water clings onto the skin; appearing as patches or droplets. If the water stays on, the spectral reflectance of skin will be altered by its presence, because now, radiation has to travel through a medium of water to reach the skin. To determine how NDSI is impacted, a data set is collected and assessed.

4.2.1 Data Collection.

In this experiment, a data set of reflectance spectra is created from mixed pixels of skin with water droplets on the top. The experiment is set up according to the mixed pixel configuration, shown in in Figure 3.5. As in Experiment 1: the distance from the pistol grip to the target measures 12.7 cm, no foreoptic are used, and the angular field-of-view measures 25°; resulting in a field-of-view of 5.63 cm in diameter.

A subject's hand is placed palm down, as flat as possible, in the center of the field-of-view; serving as the background of the pixel. Prior to each data collect, the skin sample area is washed with soap and water. Droplets of distilled water are added to the back of the hand with a pipette. For each sample, the reflectance spectrum of the pixel is measured with the FieldSpec. Between each sample, the hand is dried before continuing with the data collect. The histogram of the samples are shown in Figure 4.7, illustrating a spread of samples across the amount of water droplets. Due to the limited space on the back of the hand and the difficulty of keeping the hand in place, only six amounts are examined.

4.2.2 NDSI Evaluation.

The resulting NDSI values for the data set collected in Experiment 2 are shown in Figure 4.8 as a plot of the water droplets verse the NDSI, with error bars denoting the standard deviation. A mixed pixel of skin with 1.07 mL of water droplets results in a

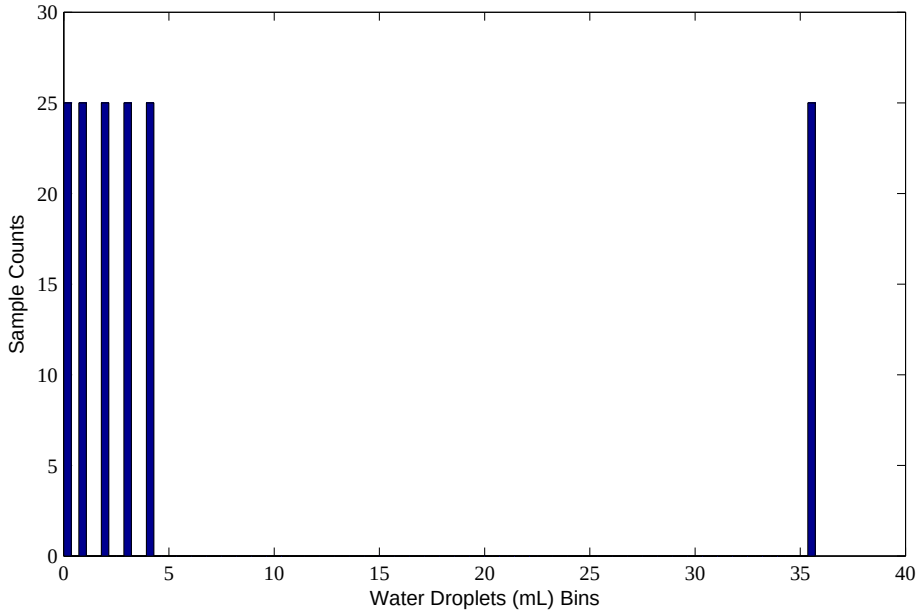

Figure 4.7: Histogram of the data set from Experiment 2 (Water Droplets). Samples more than 5 mL of water droplets are not taken due to practicality; because with additional water, the droplets rolls off the back of the hand. The collection at 35 mL resulted in a loss of over 50% water droplets.

NDSI of approximately 0.72. Doubling the amount of water droplets to 2.14 mL results in a slight change in NDSI, an increase of 0.03 to 0.75. Than NDSI tops out at approximately 0.755 with 3.21 mL and 4.28 mL of water. No higher amounts of water droplets are examined due to practicality; additional water droplets rolls off the back of the hand. For the samples at 35.71 mL of water droplets, more than half of the water is estimated to be lost, but NDSI s relatively unchanged at 0.76.

There is not a wide range of NDSI values, meaning the amount of water droplets evaluated had minimum impact on NDSI. While working with such low amounts of water, it is not surprising that NDSI is not affected. The NDSI of the subject is measured to be approximately 0.71. With a NDSI range of 0.71 to 0.75, or to 0.76 at an extreme case, the

threshold detector from Equation 2.5 only needs a upper NDSI threshold of approximately $a_2 = 0.76$ to detect all of the mixed pixels in this experiment.

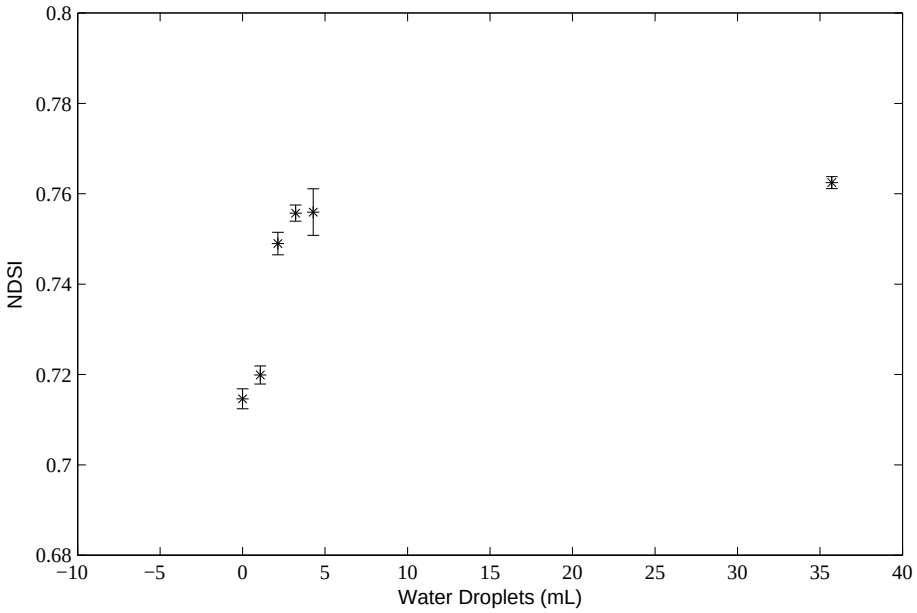

Figure 4.8: NDSIs of the data set from Experiment 2 (Water Droplet). The error bars denotes the standard deviation. NDSI is mostly invariant to water droplets with a small range of NDSI values for skin-positive pixels.

Plots of the reflectance spectra from the data set is shown in Figure 4.9. At a glance, no significant differences are seen between the spectra for the six evaluated amount of water droplets. It is interesting to note that spectra are not affected in a linear manner at the two NDSI wavelengths, such that the reflectance values should appear in the same order at both wavelengths. At $\lambda(1080)$, the reflectance ranks from highest to lowest in the order: 0 mL, 1.07 mL, 2.14 mL, 3.21 mL, 35.71 mL, and then 4.28 mL. At $\lambda(1580)$, the order is: 0 mL, 1.07 mL, 2.14 mL, 3.21 mL, 4.28 mL, and than 35.71 mL. The 35.71 mL spectrum is the outliers at both wavelengths; hypothetically, it should have the lowest reflectance, with

the highest amount of water, but it varies between the 1.07 mL and 4.28 mL spectra. This goes to show how much of the original 35.71 mL of water rolled off.

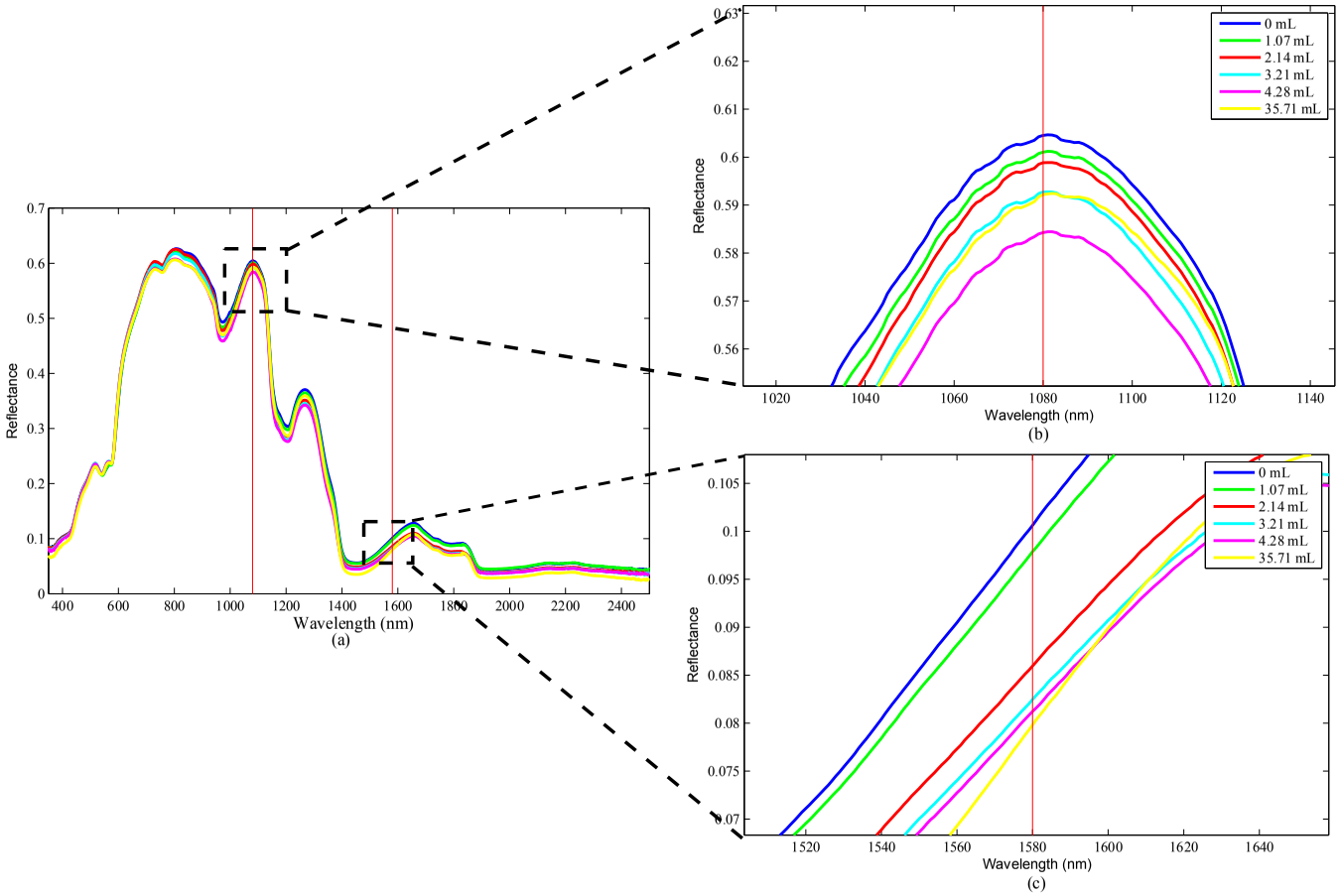

Figure 4.9: The reflectance spectra of the data set with mixed pixels of skin with water droplets; (a) Minimal variation between the spectra is apparent from a view of the full spectrum range; (b) An enlargement of the band around 1080 nm; (c) An enlargement of the band around 1580 nm. Note the inconsistent order of the reflectance between (b) and (c). The nonlinear effect of water at those two wavelengths is seen from the different changes in range.

4.3 Experiment 3 - Water Layer

The objective of the third experiment is to answer the question: How does a mixed pixel of skin under a thin layer of water impact NDSI? Radiation does not travel well through water because of exponential attenuation from absorptions and scattering [20, 37]. If the person's skin is underneath water, radiation may survive shallower depths, towards the surface of the body of water. Similar to Experiment 2, when radiation has to travel through a median of water, skin reflectance will change. To determine how NDSI is impacted, a data set is collected and assessed.

4.3.1 Data Collection.

In this experiment, a data set of reflectance spectra is created from mixed pixels of skin under a thin layer of water on top. The amount of skin in the mixed pixel is held constant, while the height of the water layer varies. The experiment is set up according to the mixed pixel configuration, shown in in Figure 3.5. As in Experiment 1 and 2: the distance from the pistol grip to the target measures 12.7 cm, no foreoptic are used, and the angular field-of-view measures 25°, resulting in a field-of-view of 5.63 cm in diameter.

A plastic container for the water is placed centered on the target area platform. A subject's hand is placed palm down, as flat as possible, in the container. Prior to each data collect, the skin sample area is washed with soap and water. The container is filled with distilled water, measuring from the top of the subject hand. For each sample, the reflectance spectrum of the pixel is measured with the FieldSpec. The histogram of the samples are shown in Figure 4.10, illustrating a spread of samples across the height of the water layer.

4.3.2 NDSI Evaluation.

The resulting NDSI values for the data set collected in Experiment 3 is shown in Figure 4.11 as a plot of the water layer height versus the NDSI, with error bars denoting the standard deviation. With no water layer present, the NDSI of just skin measures 0.74;

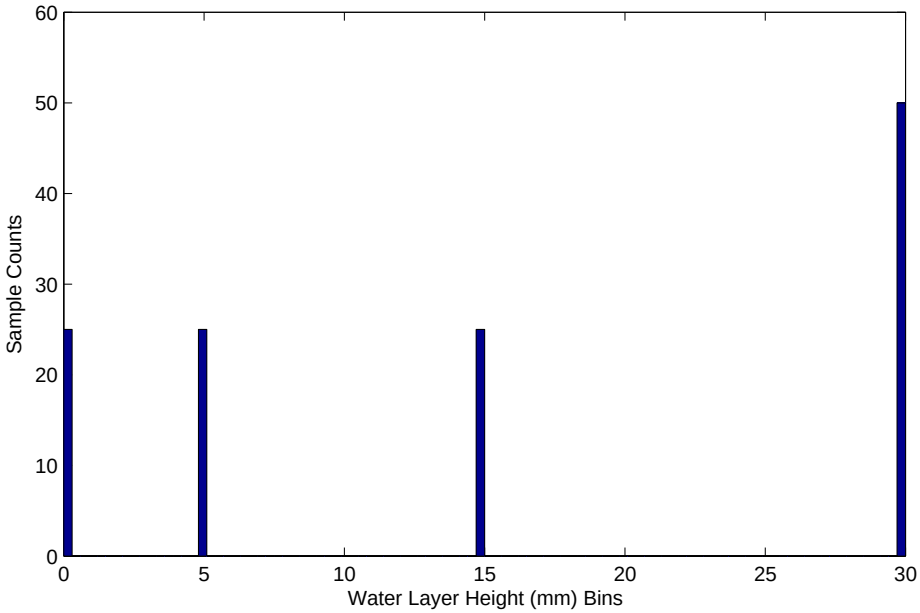

Figure 4.10: Histogram of the data set from Experiment 3 (Water Layers).

consistent with the values previous seen. Once water is added and the height of the water layer exceeds 5 mm, the resulting NDSI of approximately 0.99.

Plots of the reflectance spectra from the data set is shown in Figure 4.12. Past 1400 nm, reflectance goes completely to zero once 5 mm, or more, layer of water is introduced to the pixel; including one of the wavelength of interest: 1580 nm. With $\lambda(1580) = 0$, the NDSI function from Equation 2.2 turns into:

$$\text{NDSI} = \frac{\lambda(1080) - 0}{\lambda(1080) + 0} = \frac{\lambda(1080)}{\lambda(1080)} = 1, \tag{4.5}$$

which explains the results of 0.99.

As discussed before, water exhibits high absorbing characteristics. While two major water absorption bands exists at approximately 1500 nm and 1900 nm, there is constant absorption through the infrared region. Evidently, 5 mm of water is enough to mask the reflectance of skin in a mixed pixel. With as little as 5 mm of water, NDSI is rendered useless; meaning NDSI will fail to detect skin under any amount of water.

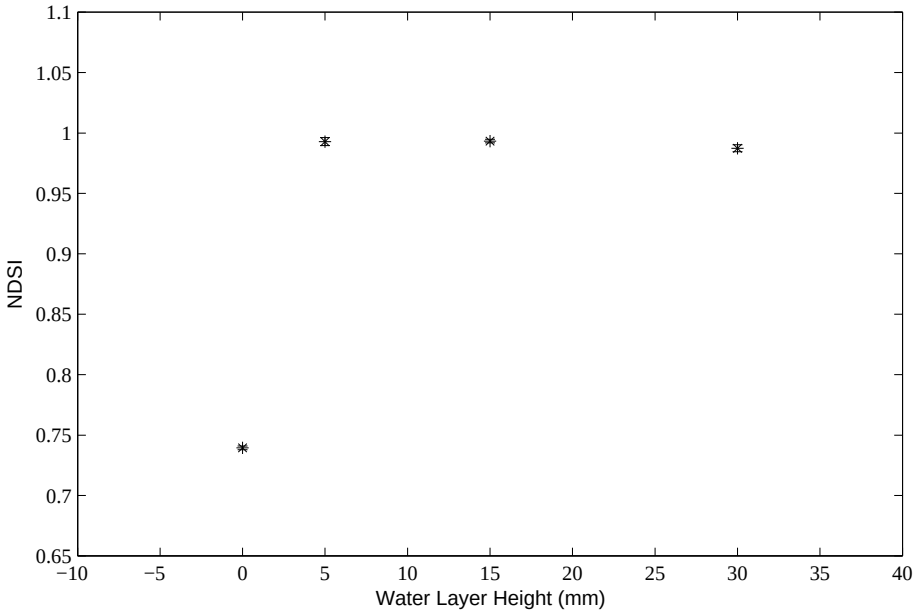

Figure 4.11: NDSIs of the data set from Experiment 2 (Water Layers). The error bars denotes the standard deviation. The NDSI of 0.74 at 0 mm is for the case of no water. Once 5 mm or more water is added, NDSI fails to function due to the lost of the second wavelength, 1580 nm, from water absorption.

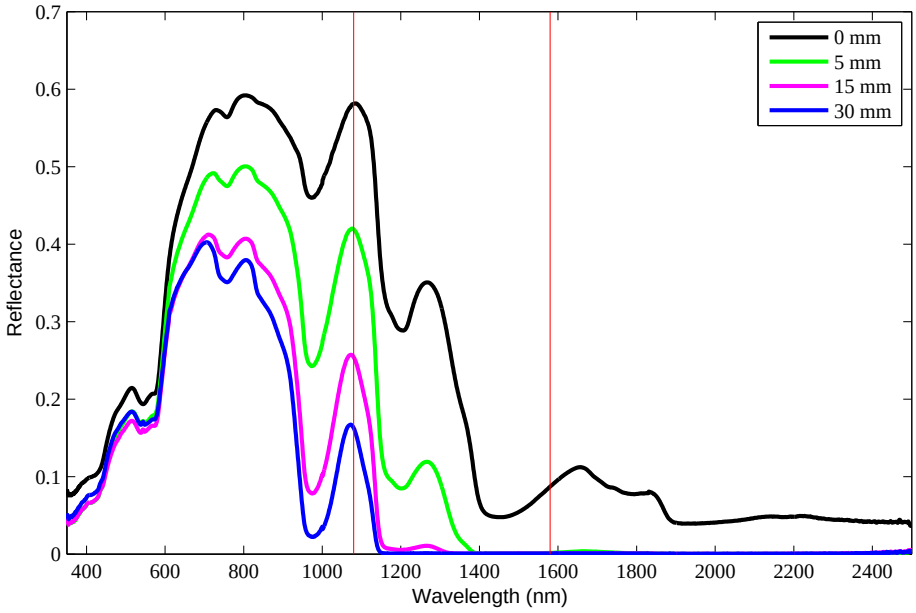

Figure 4.12: The reflectance spectra of the data set with mixed pixels of skin under a water layers. Past 1400 nm, water absorption is strong enough to occult skin reflectance, including the second NDSI wavelength, 1580 nm.

4.4 Experiment 4 - Waterlogged Skin

The objective of the forth experiment is to answer the question: How does skin that has been submerged in water impact NDSI? As discussed in Chapter 2, skin is known in absorb or take-in water; this is apparent from pruney fingers after a hot shower. Since water is one of the three major components that defines the spectral signature of skin, the increase of water content in the skin should modify it. To determine how NDSI is impacted, a data set is collected and assessed.

4.4.1 Data Collection.

In this experiment, a data set of the reflectance spectra is created from skin that has been submerged in water at varying time durations. The experiment is set up according to the spectral signature configuration, using the contact probe. To obtain waterlogged skin, a subject's hand is placed in a plastic glove filled with distilled water up past the wrist. For each sample, the contact probe is used to collect the reflectance spectrum of the lower back portion of the hand. Prior to each data collect, the hand is washed with soap and water. Between each sample, the hand is dried before continuing with the data collect. The histogram of the samples are shown in Figure 4.13, illustrating a spread of samples across time durations.

4.4.2 NDSI Evaluation.

The resulting NDSI values for the data set collected in Experiment 4 is shown in Figure 4.14 as a plot of the time duration verse the NDSI, with error bars denoting the standard deviation and a fitted linear line for reference. The mean NDSI of the dry skin samples is approximately 0.707, consistent with previous results. Besides that, a pattern is not apparent between the time durations and NDSI value. The highest NDSI is 0.757 at the time of 6300 s, but the next highest is 0.746 at the time of 300 s. Between 300 s and 6300 s, NDSI varies with a low of 0.706 at 600 s. Using the threshold detector from

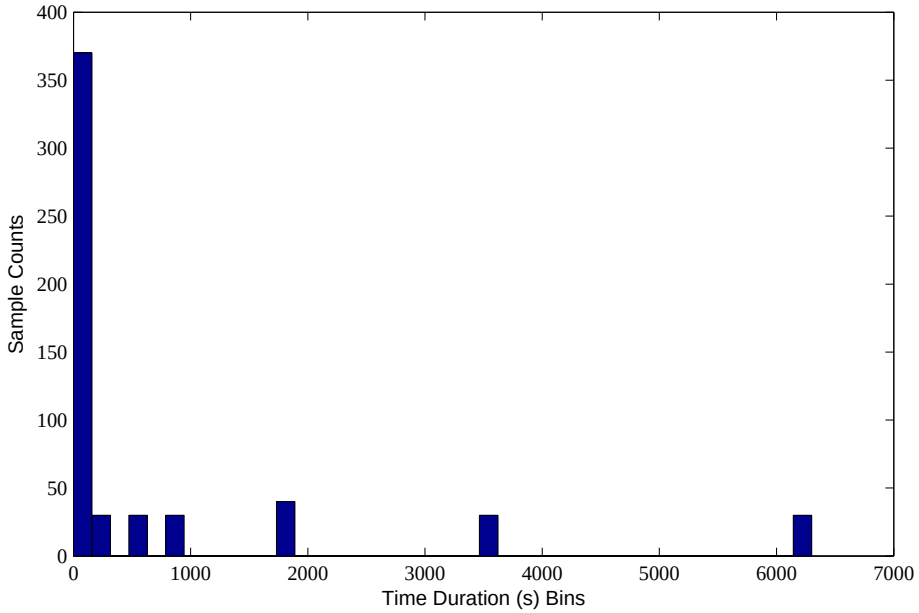

Figure 4.13: Histogram of the data set from Experiment 4 (Waterlogged Skin).

Equation 2.5, all of the skin samples from this experimental can be detected with a narrow threshold of 0.706 to 0.757.

Plots of the reflectance spectra from the data set is shown in Figure 4.15. Most of the variations between the spectra occurs in the region of 800 nm and 1080 nm, while the spectra around 1580 nm stays relative constant. Also, similar to Experiment 2, the order of reflectance are inconsistent between 1080 nm and 1580 nm. As suspected before from Experiment 1, water affects the two NDSI wavelength in a nonlinear manner.

Overall, the variation between the spectra is minimal; mostly likely, an significant amount of water is absorbed in the evaluated time duration. In a study done on in vivo hydration measurements, a method was proposed to utilize the water absorption band in the region of 960 nm to 1700 nm [2]. There is a correlation between water and absorption, more water means more absorption. The area under the reflectance spectrum from 960 nm to 1700 nm should correspond to water content, more water means a lower reflectance. The plot of the area values are shown in Figure 4.16. Based on the premise of this

measurement method, area should go down as time duration increase if more water is absorbed over time. However, the data does not support this method; area goes up, down, and up again between 0 s to 6300 s. Either this method does not work or a very little amount of water is absorbed by the skin in the evaluated duration.

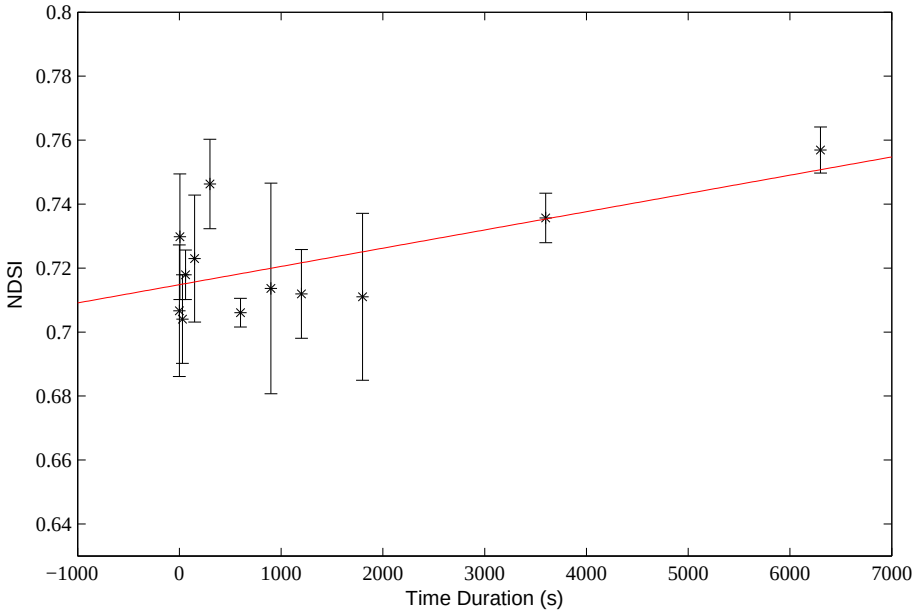

Figure 4.14: NDSIs of the data set from Experiment 4 (Waterlogged Skin). The error bars denotes the standard deviation. The red line is a linear fitted line for reference. There is not a consistent pattern between time duration and NDSI. Overall, NDSI remain relatively constant around 0.72 and invariant to the temporal affect of waterlogged skin.

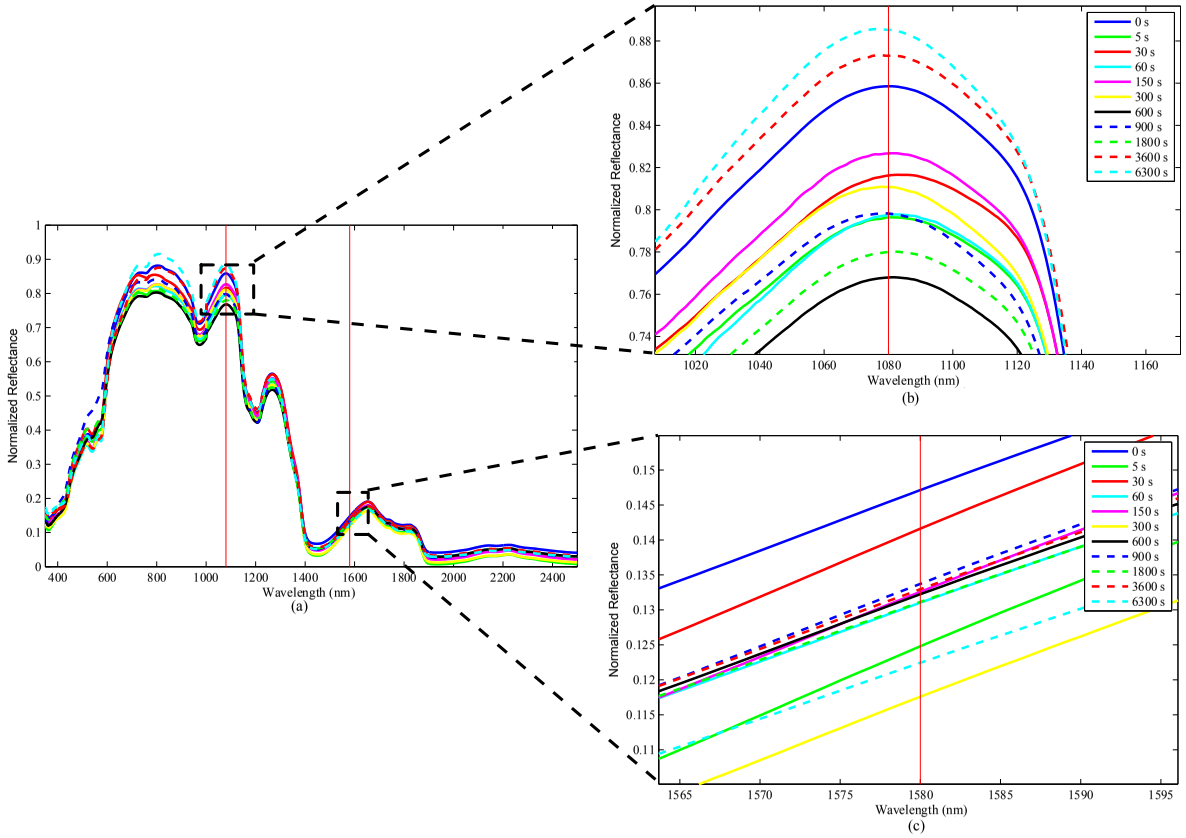

Figure 4.15: The reflectance spectra of the data set with waterlogged skin; (a) Minimal variation between the spectra is apparent from a view of the full spectrum range except in band around 800 nm and 1080 nm; (b) An enlargement of the band around 1080 nm; (c) An enlargement of the band around 1580 nm. Note the inconsistent order of the reflectance between (b) and (c). The nonlinear effect of water at those two wavelengths is seen from the different changes in range.

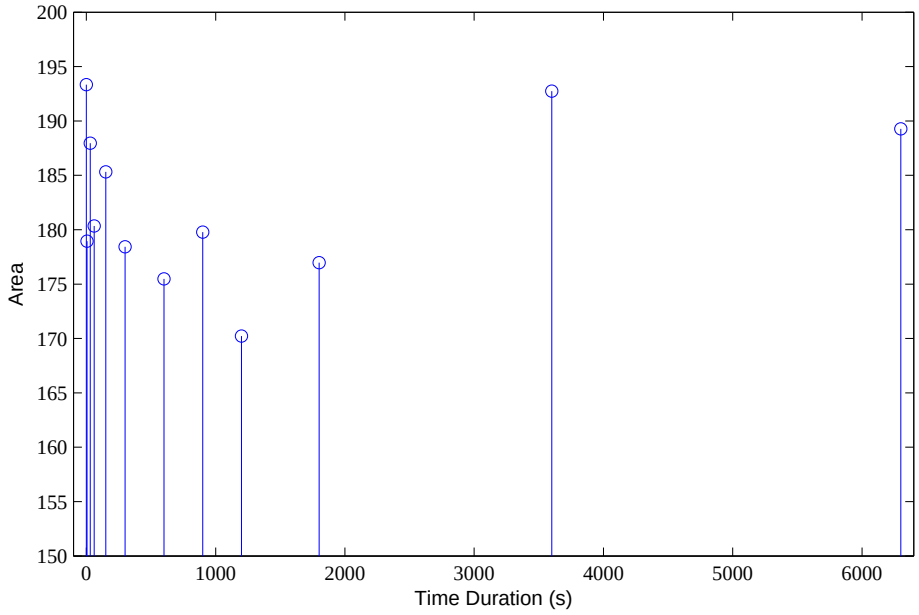

Figure 4.16: A method for hydration calculation [2]. The area under the spectrum in the region of 960 nm to 1700 nm is plotted against time duration. The premise of this method is that more water meaning a lower reflectance, which results in a smaller area. The area remains relatively constant across the time duration; either this method does not work or an insignificant amount of water is absopred by skin.

4.5 Chapter Summary

In this chapter, the robustness of NDSI in aquatic environments starts to become apparent from the results of the experiment. In the instances of water droplets and waterlogged skin, NDSI is virtually not affected. With mixed pixels of water background, NDSI correlates to the amount of skin in the pixel. At the extreme end, the presence of water can render NDSI unusable, as in the case of water layers.

V. Conclusion

5.1 Thesis Summary

The goal of this thesis is to assess how robust Normalized Difference Skin Index (NDSI) is in an aquatic environment. An hypothetical scenario was presented in Chapter 1, which serve the basis for the creation of four questions, the problem statements of this thesis:

1. Water Background. How does a mixed pixel of skin with water in the background impact NDSI?

2. Water Droplets. How does a mixed pixel of skin with water droplets on surface of the skin impact NDSI?

3. Water Layer. How does a mixed pixel of skin under a thin layer of water impact NDSI?

4. Waterlogged Skin. How does skin that has been submerged in water impact NDSI?

Experiments were created to emulate the hypothetical scenario in a laboratory setting for data collection. NDSI was computed for each of the data sets to evaluate how water impacts NDSI, in terms of the four posed questions. For a threshold-based detection system, the range of the threshold has to be minimized to prevent false detections. Therefore, to use NDSI as the threshold, the range of skin values has to be minimal.

The purpose of Experiment 1 is to assess the impact of water in the background of a skin mixed pixel. The abundance of skin in the pixel was varied from 100% to 0%, the rest being water. This resulted in NDSI values in the range of approximately 0.7 to 1. There is a correlation between NDSI and the skin percentage in the mixed pixel. When the amount of skin in the pixel decreases, water becomes more dominate in the reflectance of

the mixed pixel. This impacts the two NDSI wavelength in an nonlinear manner, changing the relationship between the two parameters of the function and invalidates it. With the rules based skin detector and Nunez's thresholds, 0.65703 to 0.76779, only mixed pixels with 64% skin or more could be identified.

The purpose of Experiment 2 is to assess the impact of water droplets on the surface of skin. Various amounts of water were evaluated, however, the results did not show any difference. NDSI held consistent values across all of the assessed amounts of water. A possible explanation is that amount of water present in the mixed pixel was probably insignificant.

The purpose of Experiment 3 is to assess the impact of water layers on skin. The height of the water layer was varied from 5 mm to 30 mm. Radiation is known to travel poorly through a medium of water, which is apparent in the results. At a shallow depth of 5 mm, NDSI was rendered useless with the lost of the second NDSI wavelength at 1580 nm. The absorption characteristic of water is strong enough to drive the reflectance at 1580 nm to zero.

The purpose of Experiment 4 is to assess the impact of water absorbed by the skin. Skin was submerged in water for different time durations that varied from a quick dip into the water to 6300 s. The resulting NDSI values did not show a major difference between the evaluated times. A novel technique was applied to gage the amount of water absorbed by the skin. The results of this hydration measurement were also constant between the evaluated times. Similar to Experiment 2, the amount of water absorbed by the skin, hence present in a pixel, was probably insignificant.

5.2 Future Work

A challenge to most line of research is the transition from the laboratory into the real world environment. The experiments devised in this thesis are just the start of evaluating NDSI robustness.

For future work, more real world variability should be introduced into the experiments, such as: increasing stand-off distance, factoring in atmospheric influences or illumination, amount, distribution, types of water, or using dermatological products. In the mixed pixel configuration, the spectroradiometer was at most 13 cm from the target. Realistically, this distance will never be seen and the dismount will be much further away from the sensor. As stand-off distance increases, atmospheric conditions and illumination becomes more of a concern. In the experiments, the influence of the atmospheric was effectively minimized to scope the thesis. But once there is a greater distance between the sensor and target, other materials such as the water-vapor or carbon dioxide in the atmosphere are introduced into the field-of-view. In the experiments, the illumination incident on the target was measured with white reference panels. However, in real life, white reference panels can not be placed everywhere a dismount can be found. While there are methods available to obtain reflectance measurements without the use of white reference panels, the results of these methods are still far from perfection; there may not enough information for the spectrum to be identifiable based on spectral signatures. As mentioned in Chapter 3, many types of water can be encountered on this planet, also, at amounts vastly greater than the ones tested in the experiments. Since only distilled water was used, results could differ significantly if the experiments were repeated using other types of water. Before each data collection, the skin sample area was washed with soap and water in efforts to remove variability; operationally, this may not be the case. If the dismount is consciously avoiding detection, their skin may be painted to camouflage with the environment. How this paint or other dermatological products, such as lotion, influences the spectral signature of skin

has not been evaluated in this thesis. For verification and validation purposes, hyperspectral images of dismount in bodies of water should be collected.

Appendix A: Water Background Data Sets

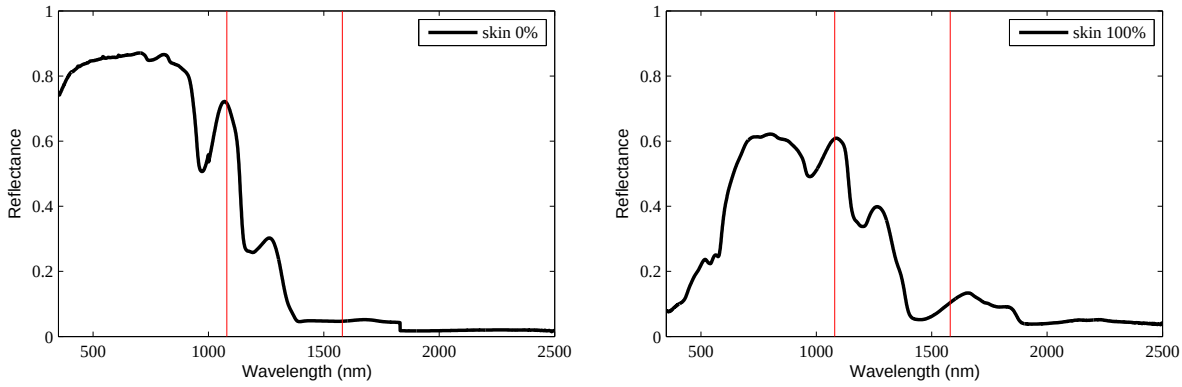

(a) (b)

Figure A.1: The average spectral reflectance of the (a) 0% skin and (b) 100% skin samples of Experiment 1.

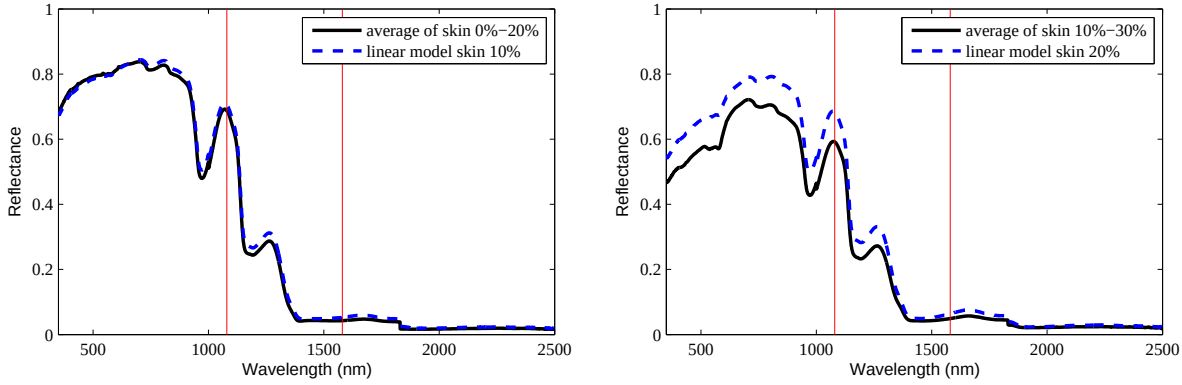

(a) (b)

Figure A.2: The average spectral reflectance of samples from of Experiment 1 compared to a linear mixing model (a) 10% and (b) 20%.

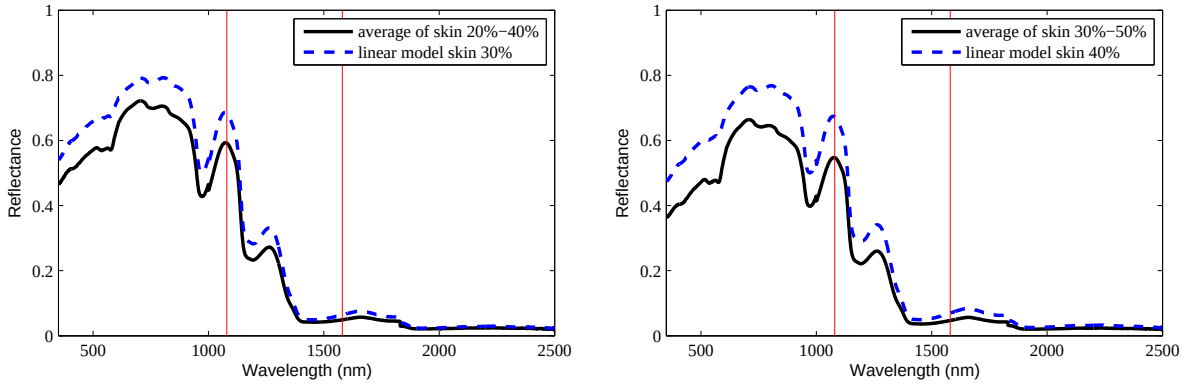

(a) (b)

Figure A.3: The average spectral reflectance of samples from of Experiment 1 compared to a linear mixing model (a) 30% and (b) 40%.

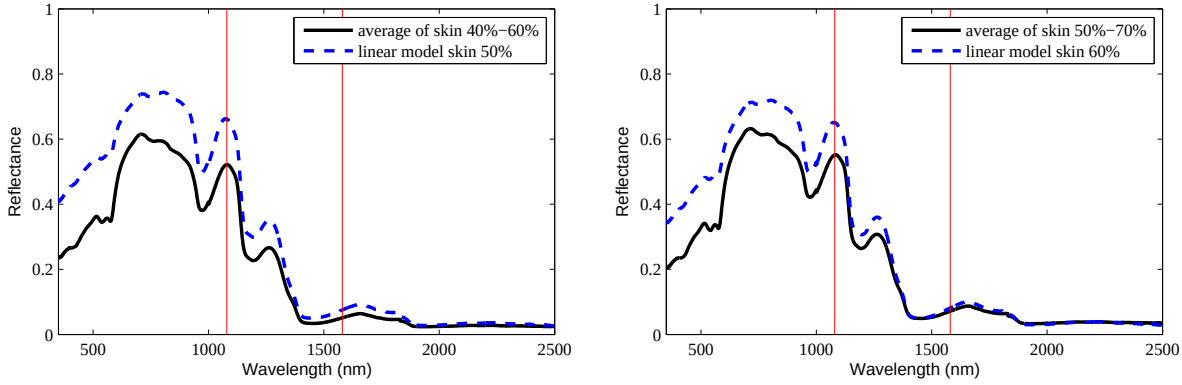

(a) (b)

Figure A.4: The average spectral reflectance of samples from of Experiment 1 compared to a linear mixing model (a) 50% and (b) 60%.

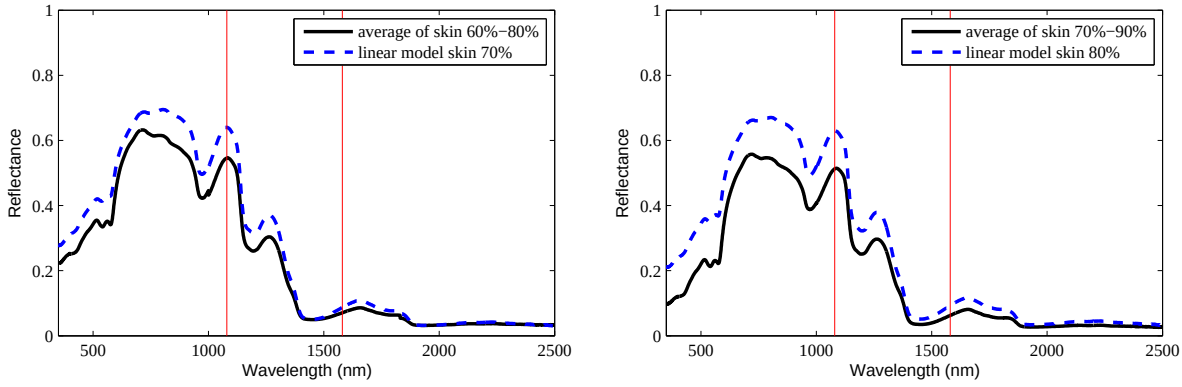

(a) (b)

Figure A.5: The average spectral reflectance of samples from of Experiment 1 compared to a linear mixing model (a) 70% and (b) 80%.

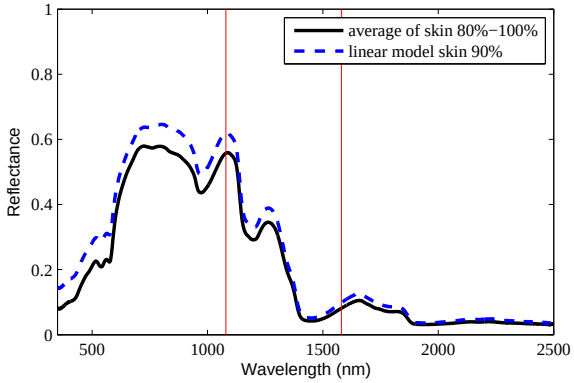

Figure A.6: The average spectral reflectance of samples from of Experiment 1 compared to a linear mixing model 90%.

Appendix B: Cloth Background Data Sets

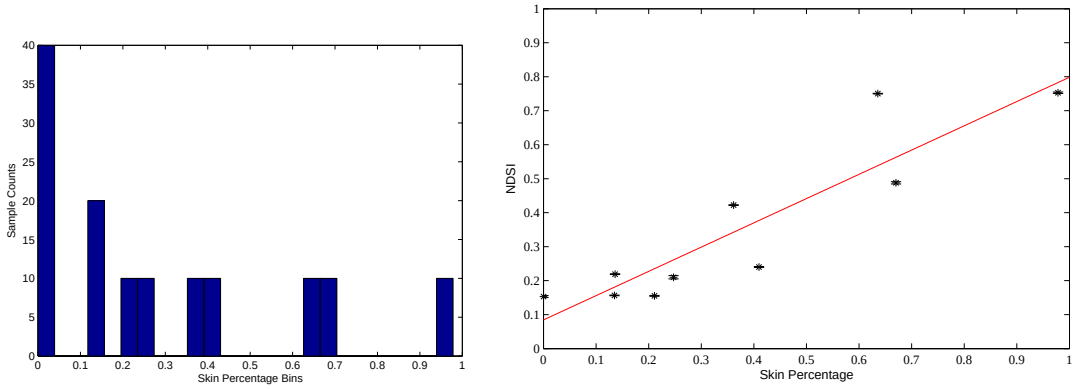

(a) (b)

Figure B.1: A data set of reflectance spectra is created from mixed pixels of skin with cloth in the background; (a) Histogram of data set; (b) NDSI of the data set.

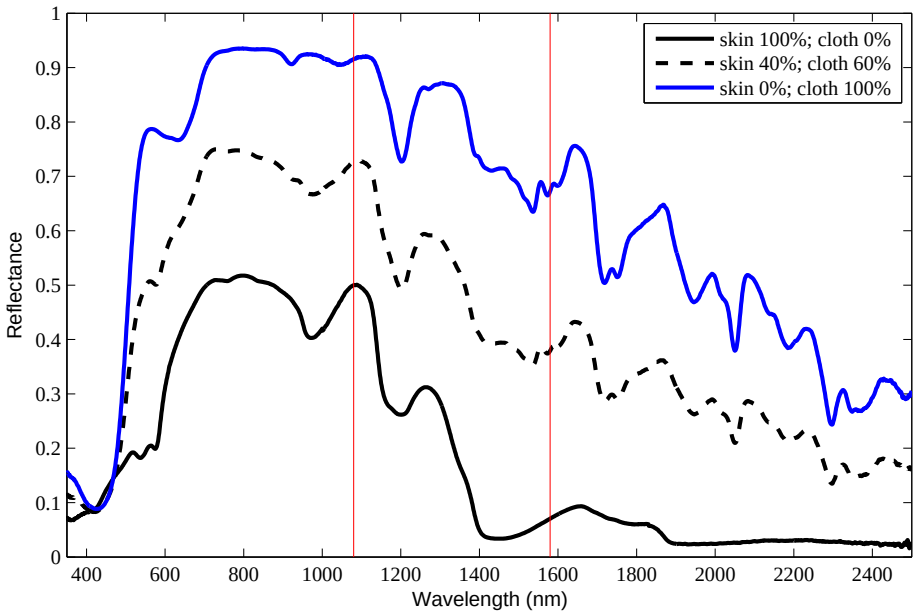

Figure B.2: Three averaged reflectance spectra from the Cloth Background data set: 100% skin (black), 100% cloth (blue), 50% skin (dashed).

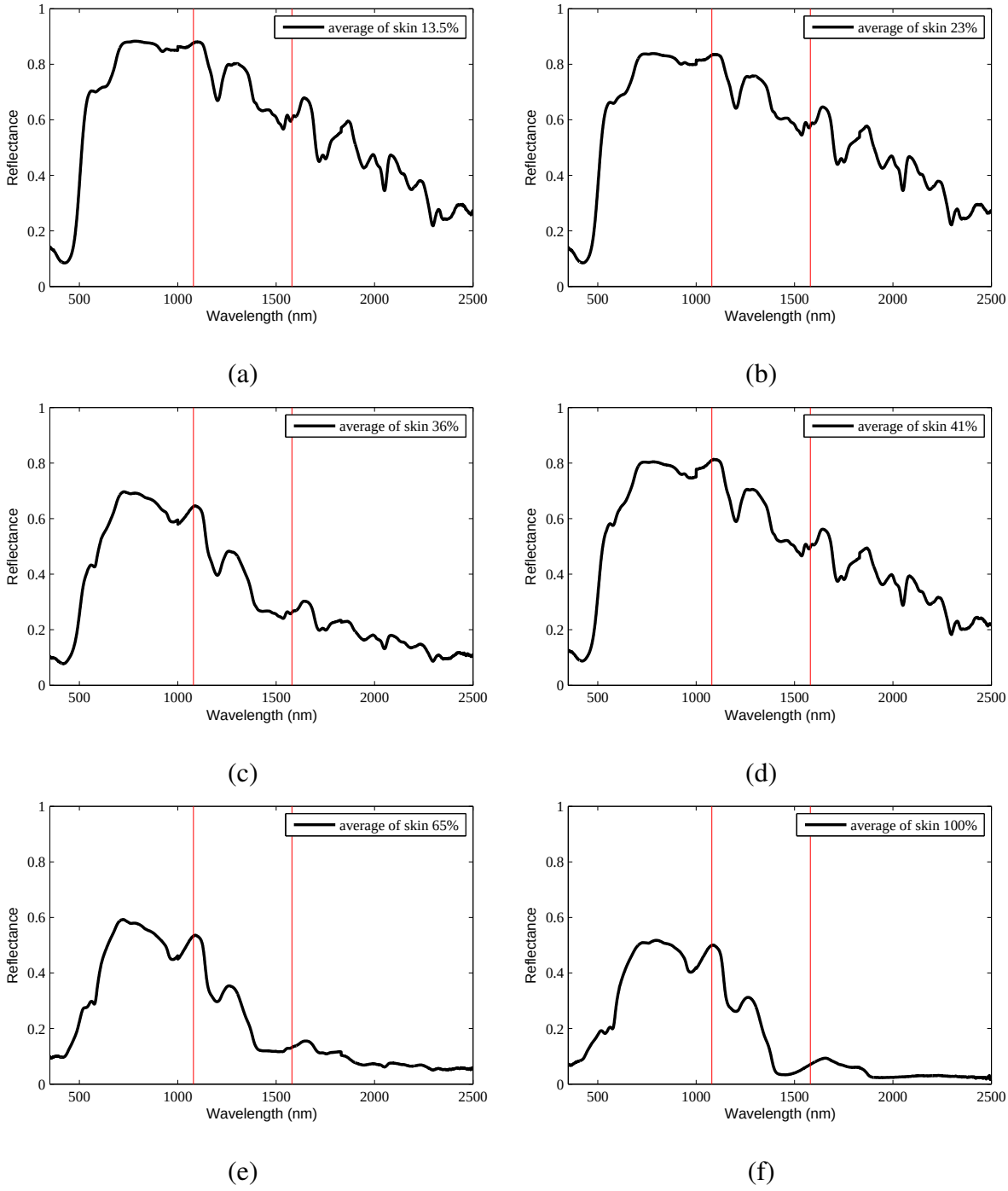

Figure B.3: The average spectral reflectance of samples from of Experiment 1 with cloth background; (a) 13.5% (b) 23% (c) 36% (d) 41% (e) 65% (f) 100%

Appendix C: Sand Background Data Sets

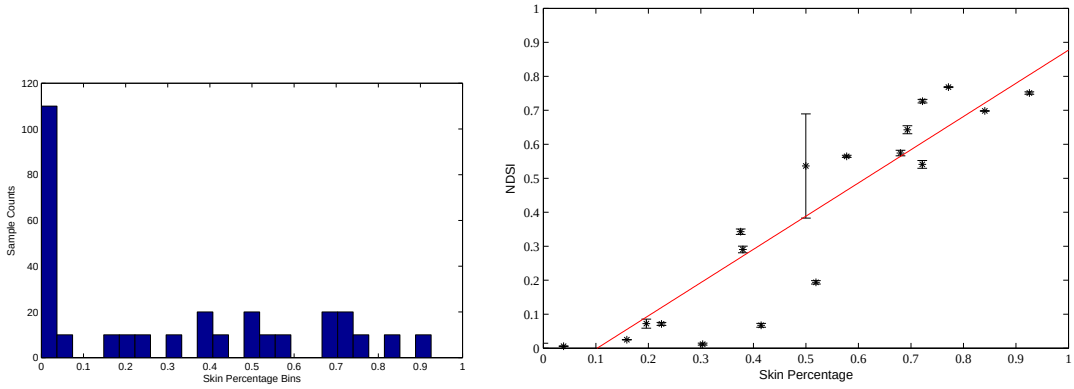

(a) (b)

Figure C.1: A data set of reflectance spectra is created from mixed pixels of skin with sand in the background; (a) Histogram of data set; (b) NDSI of the data set.

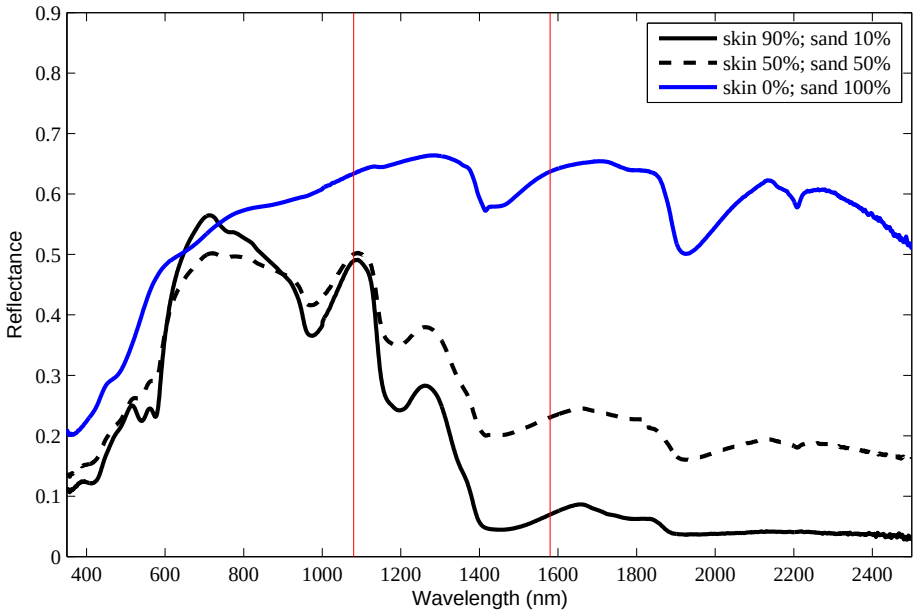

Figure C.2: Three averaged reflectance spectra from the Sand Background data set: 100% skin (black), 100% sand (blue), 50% skin (dashed).

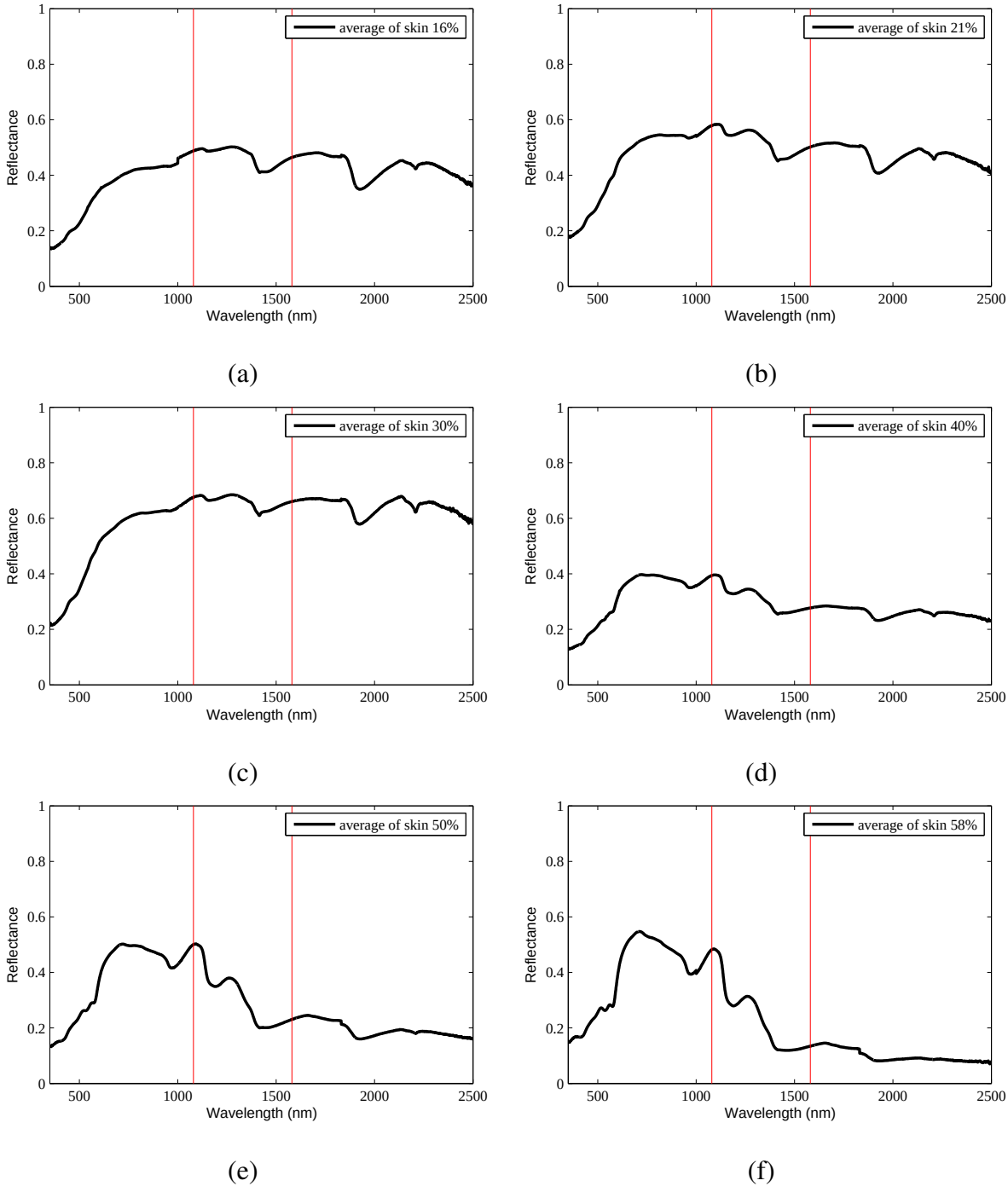

Figure C.3: The average spectral reflectance of samples from of Experiment 1 with sand background; (a) 16% (b) 21% (c) 30% (d) 40% (e) 50% (f) 58%

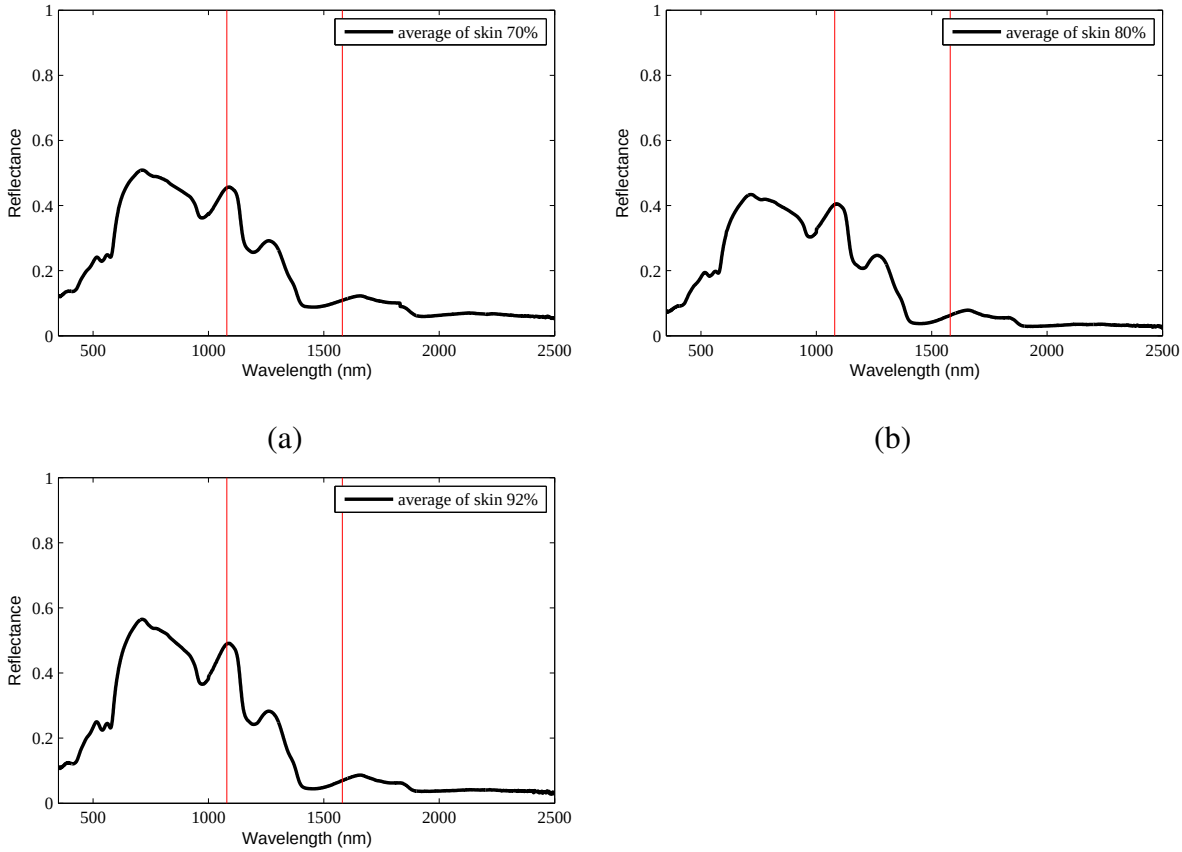

Figure C.4: The average spectral reflectance of samples from of Experiment 1 with sand background; (a) 70% (b) 80% (c) 92%

Appendix D: Grass Background Data Sets

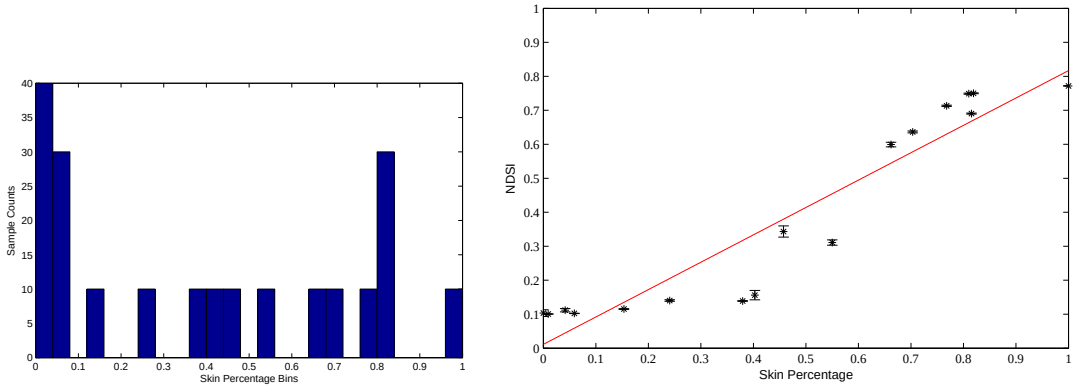

(a) (b)

Figure D.1: A data set of reflectance spectra is created from mixed pixels of skin with grass in the background; (a) Histogram of data set; (b) NDSI of the data set.

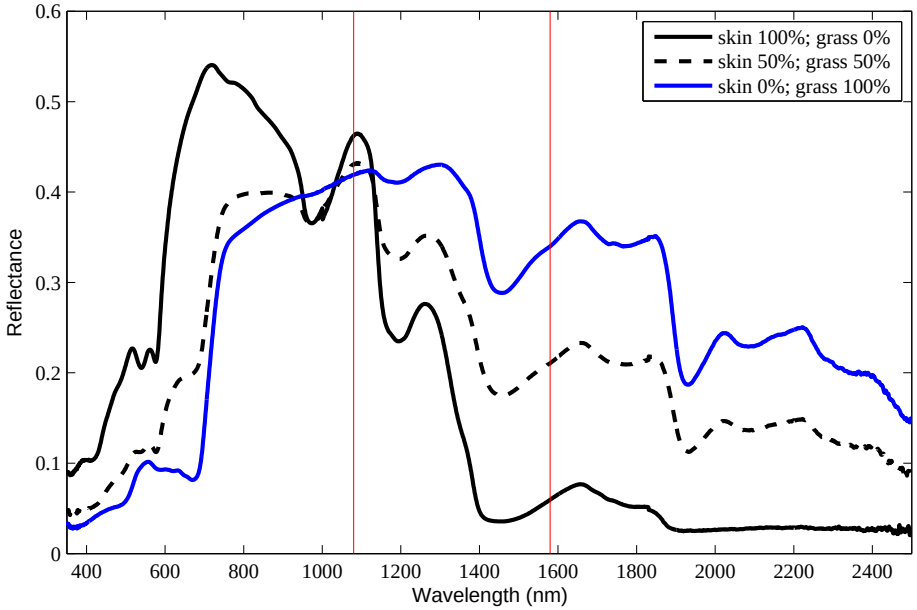

Figure D.2: Three averaged reflectance spectra from the Grass Background data set: 100% skin (black), 100% grass (blue), 50% skin (dashed).

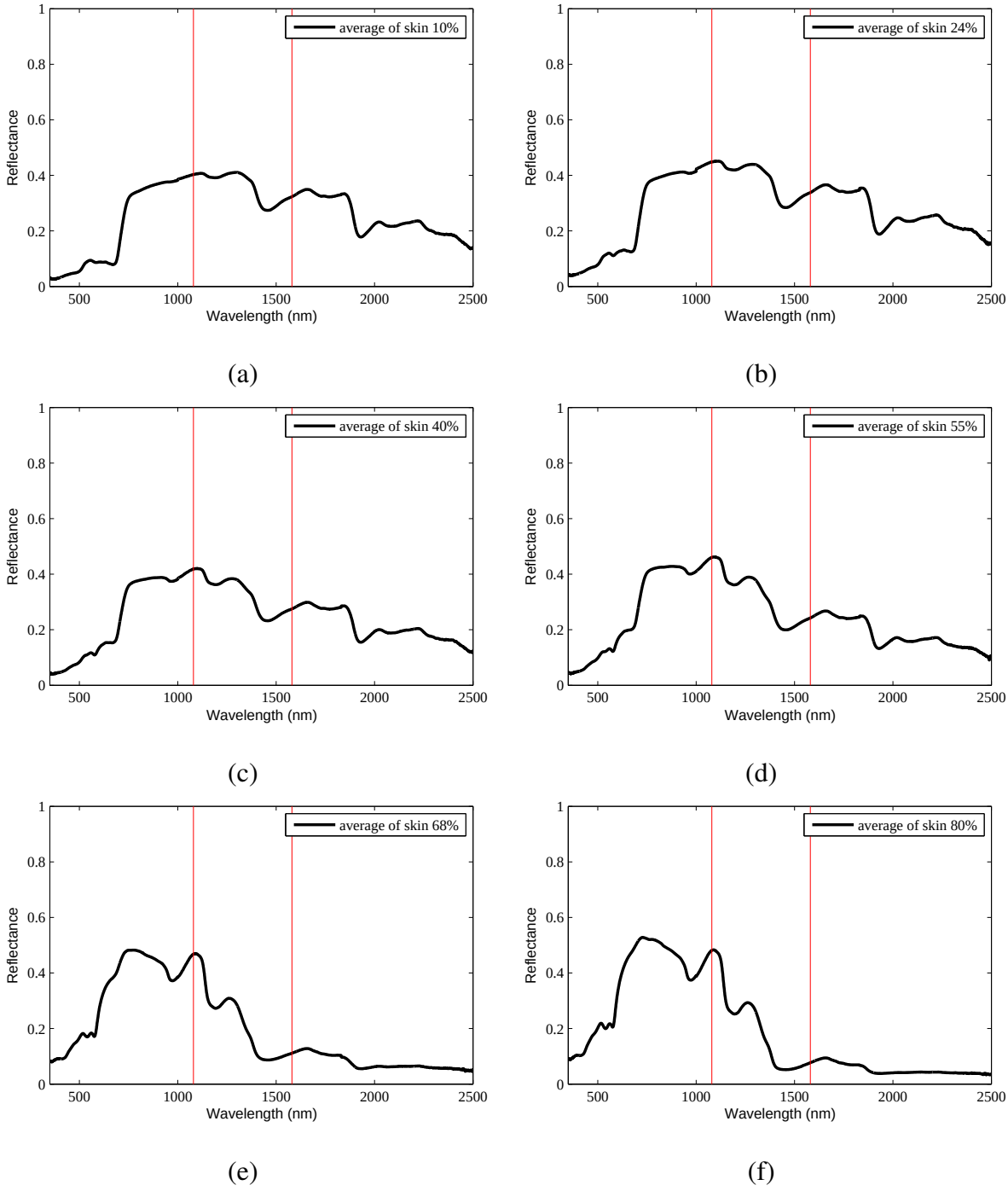

Figure D.3: The average spectral reflectance of samples from of Experiment 1 with grass background; (a) 10% (b) 24% (c) 40% (d) 55% (e) 68% (f) 80%

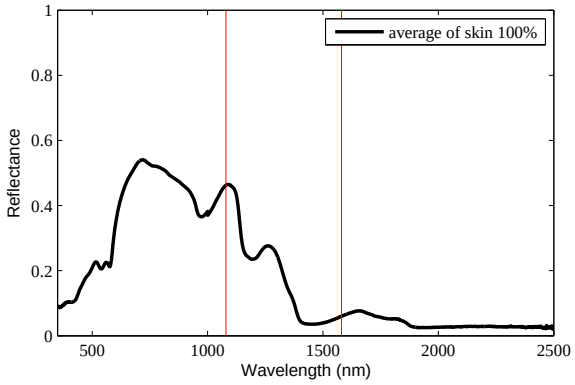

(a)

Figure D.4: The average spectral reflectance of samples from of Experiment 1 with grass background; (a) 100%

Bibliography

[1] "The Hydrologic Cycle Pamphlet", 1984.

[2] Attas, Michael, Trevor Posthumus, Bernie Schattka, Michael Sowa, Henry Mantsch, and Shuliang Zhang. "Long-wavelength near-infrared spectroscopic imaging for in-vivo skin hydration measurements". *Vibrational Spectroscopy*, 28(1):37–43, 2/28 2002.

[3] Beisley, Andrew P. "Spectral Detection of Human Skin in VIS-SWIR Hyperspectral Imagery without Radiometric Calibration". 2012.

[4] Borengasser, Marcus, William S. Hungate, and Russell Watkins. *Hyperspectral remote sensing: principles and applications*. Crc Press, 2010.

[5] Boundless. *Anatomy and Physiology*. Boundless Learning, 2013. URL http://books.google.com/books?id=7avpAAAAQBAJ&printsec=frontcover&dq=anatomy+and+physiology&hl=en&sa=X&ei=7MztUtWfAYON2gWfzYHgDA&ved=0CCoQ6AEwAA#v=onepage&q=anatomy%20and%20physiology&f=false.

[6] Brooks, Adam L. "Improved multispectral skin detection and its application to search space reduction for dismount detection based on histograms of oriented gradients". 2010.

[7] Clark, Jeffrey D. "Distributed Spacing Stochastic Feature Selection and its Application to Textile Classification". 2011.

[8] Costin, Gertrude-E and Vincent J. Hearing. "Human skin pigmentation: melanocytes modulate skin color in response to stress". *The FASEB Journal*, 21(4):976–994, 2007.

[9] Egawa, Mariko, Tetsuji Hirao, and Motoji Takahashi. "In vivo estimation of stratum corneum thickness from water concentration profiles obtained with Raman spectroscopy". *Acta Dermato-Venereologica*, 87(1):4–8, 2007.

[10] Eismann, Michael T. "Hyperspectral remote sensing". SPIE, 2012.

[11] Freeman, Andrew M. "Dismount Threat Recognition through Automatic Pose Identification". 2012.

[12] Gao, Bo-Cai. "NDWI A Normalized Difference Water Index for Remote Sensing of Vegetation Liquid Water from Space". *Remote Sensing of Environment*, 58(3):257–266, 1996.

[13] Gao, Bo-Cai, Marcos J. Montes, Curtiss O. Davis, and Alexander FH Goetz. "Atmospheric correction algorithms for hyperspectral remote sensing data of land and ocean". *Remote Sensing of Environment*, 113:S17–S24, 2009.

[14] Gleick, Peter H. "The human right to water". *Water Policy*, 1(5):487–503, 1998.

[15] Griffin, Michael K. "Compensation of hyperspectral data for atmospheric effects". *Lincoln Laboratory Journal*, 14(1):29–54, 2003.

[16] Jacques, Steven L. "Skin optics". *Oregon Medical Laser Center News*, 1998(1):1–9, 1998.

[17] Jones, Byran F. "A reappraisal of the use of infrared thermal image analysis in medicine". *Medical Imaging, IEEE Transactions on*, 17(6):1019–1027, 1998.

[18] Keshava, N. and J. F. Mustard. "Spectral unmixing". *Signal Processing Magazine, IEEE*, 19(1):44–57, 2002. ID: 1.

[19] Keshava, Nirmal. "A survey of spectral unmixing algorithms". *Lincoln Laboratory Journal*, 14(1):55–78, 2003.

[20] Kocak, Donna M., Fraser R. Dalgleish, Frank M. Caimi, and Yoav Y. Schechner. "A focus on recent developments and trends in underwater imaging". *Marine Technology Society Journal*, 42(1):52–67, 2008.

[21] Kolarsick, Paul AJ, Maria Ann Kolarsick, and Carolyn Goodwin. "Anatomy and Physiology of the Skin". *Journal of the Dermatology Nurses' Association*, 3(4):203–213, 2011.

[22] Kou, Linhong, Daniel Labrie, and Petr Chylek. "Refractive indices of water and ice in the 0.65-to 2.5-m spectral range". *Applied Optics*, 32(19):3531–3540, 1993.

[23] Lesser, MP and CD Mobley. "Bathymetry, water optical properties, and benthic classification of coral reefs using hyperspectral remote sensing imagery". *Coral Reefs*, 26(4):819–829, 2007.

[24] Madison, Kathi C. "Barrier function of the skin: "la raison d'łtre" of the epidermis". *Journal of Investigative Dermatology*, 121(2):231–241, 2003.

[25] Manolakis, Dimitris, David Marden, and Gary A. Shaw. "Hyperspectral image processing for automatic target detection applications". *Lincoln Laboratory Journal*, 14(1):79–116, 2003.

[26] Marks, Ronald and Peter A. Payne. *Bioengineering and the Skin*. Springer, 1981.

[27] Matts, PJ, PJ Dykes, and R. Marks. "The distribution of melanin in skin determined in vivo". *British Journal of Dermatology*, 156(4):620–628, 2007.

[28] ASD Inc. “FieldSpec 3 User Manual”, 2010.

[29] National Search and Rescue Committee. “Land Search and Rescue Addendum to the National Search and Rescue Supplement to the International Aeronautical and Maritime Search and Rescue Manual”.

[30] Office of Inspector General. *A Review of Remote Surveillance Technology Along U.S. Land Borders*. Technical Report OIG-06-15, Department of Homeland Security, 2005. URL http://www.oig.dhs.gov/assets/Mgmt/OIG_06-15_Dec05.pdf.

[31] United States Environmental Protection Agency. “Waters (By Type)”, 2013.

[32] World Health Organization. *Guidelines for drinking-water quality: recommendations*, volume 1. World Health Organization, 2004.

[33] Mocci, F., A. Serra, and G. A. Corrias. “Psychological factors and visual fatigue in working with video display terminals”. *Occupational and environmental medicine*, 58(4):267–271, Apr 2001. LR: 20130915; JID: 9422759; OID: NLM: PMC1740121; ppublish.

[34] Nakagawa, Noriaki, Masayuki Matsumoto, and Shingo Sakai. “In vivo measurement of the water content in the dermis by confocal Raman spectroscopy”. *Skin Research and Technology*, 16(2):137–141, 2009.

[35] Nunez, Abel S. “A physical model of human skin and its application for search and rescue”. 2009.

[36] Pellacani, Giovanni and Stefania Seidenari. “Variations in facial skin thickness and echogenicity with site and age.” *Acta Dermato-Venereologica*, 79(5), 1999.

[37] Schettini, Raimondo and Silvia Corchs. “Underwater image processing: state of the art of restoration and image enhancement methods”. *EURASIP Journal on Advances in Signal Processing*, 2010:14, 2010.

[38] Sharifahmadian, Ershad and Shahram Latifi. “Advanced hyperspectral remote sensing for target detection”. *Systems Engineering (ICSEng), 2011 21st International Conference on*, 200–205. IEEE, 2011.

[39] Shaw, Gary A. and Hsiao hua K. Burke. “Spectral imaging for remote sensing”. *Lincoln Laboratory Journal*, 14(1):3–28, 2003.

[40] Shuster, SAM, Martin M. Black, and Eva McVitie. “The influence of age and sex on skin thickness, skin collagen and density”. *British Journal of Dermatology*, 93(6):639–643, 1975.

[41] Szalma, J. L., J. S. Warm, G. Matthews, W. N. Dember, E. M. Weiler, A. Meier, and F. T. Eggemeier. “Effects of sensory modality and task duration on performance, workload, and stress in sustained attention”. *Human factors*, 46(2):219–233, Summer 2004. LR: 20061115; JID: 0374660; ppublish.

[42] Warner, Ronald R., Mark C. Myers, and Dennis A. Taylor. “Electron probe analysis of human skin: determination of the water concentration profile”. *Journal of investigative dermatology*, 90(2):218–224, 1988.

REPORT DOCUMENTATION PAGE

Form Approved
OMB No. 0704-0188

The public reporting burden for this collection of information is estimated to average 1 hour per response, including the time for reviewing instructions, searching existing data sources, gathering and maintaining the data needed, and completing and reviewing the collection of information. Send comments regarding this burden estimate or any other aspect of this collection of information, including suggestions for reducing the burden, to Department of Defense, Washington Headquarters Services, Directorate for Information Operations and Reports (0704-0188), 1215 Jefferson Davis Highway, Suite 1204, Arlington, VA 22202-4302. Respondents should be aware that notwithstanding any other provision of law, no person shall be subject to any penalty for failing to comply with a collection of information if it does not display a currently valid OMB control number.
PLEASE DO NOT RETURN YOUR FORM TO THE ABOVE ADDRESS.

1. REPORT DATE *(DD-MM-YYYY)*	2. REPORT TYPE	3. DATES COVERED *(From - To)*
27-03-2014	Master's Thesis	October 2012 - March 2014

4. TITLE AND SUBTITLE
An Assessment of Normalized Difference Skin Index Robustness in Aquatic Environments

5a. CONTRACT NUMBER

5b. GRANT NUMBER

5c. PROGRAM ELEMENT NUMBER

6. AUTHOR(S)
Chan, Alice W, First Lieutenant, USAF

5d. PROJECT NUMBER
JON 14G282

5e. TASK NUMBER

5f. WORK UNIT NUMBER

7. PERFORMING ORGANIZATION NAME(S) AND ADDRESS(ES)
Air Force Institute of Technology
Graduate School of Engineering and Management (AFIT/EN)
2950 Hobson Way
Wright-Patterson AFB OH 45433-7765

8. PERFORMING ORGANIZATION REPORT NUMBER
AFIT-ENG-14-M-17

9. SPONSORING/MONITORING AGENCY NAME(S) AND ADDRESS(ES)
Air Force Research Laboratories
711th Human Performance Wing
2800 Q Street, Bldg 824
Wright Patterson AFB, OH 45433
Dr Darrell F. Lochtefeld, Lead Scientist, darrell.lochtefeld@us.af.mil

10. SPONSOR/MONITOR'S ACRONYM(S)
AFRL/RHXBA

11. SPONSOR/MONITOR'S REPORT NUMBER(S)

12. DISTRIBUTION/AVAILABILITY STATEMENT
Distrubution Statement A: Approved for Public Release; Distribution Unlimited
DESTRUCTION NOTICE - For unclassied, limited documents, destroy by any method that will prevent disclosure of contents or reconstruction of document.

13. SUPPLEMENTARY NOTES
This work is declared a work of the U.S. Government and is not subject to copyright protection in the United States.

14. ABSTRACT
The Normalized Difference Skin Index (NDSI) is a numeric value generated from two wavelengths of the electromagnetic spectrum, a feature that can be utilized for a dismount detection system. In efforts to achieve an operational system, the robustness of NDSI has to be explored for aquatic environments. Experiments were devised to emulate scenarios that may arise between skin and water in a pixel of a hyperspectral image. With a mixed pixel of skin with water in the background, the spread of NDSI values were within a range defined by previous research until 64% or less of the pixel constituted skin. With a mixed pixel of skin with water droplets, the evaluated amount of water had negligible impact on NDSI. A mixed pixel of skin under a thin layer of water rendered NDSI useless with a shallow depth of 5 mm; water layers prove to be extremely detrimental to NDSI. Also, the temporal factor of water absorption by skin was assessed. Within the evaluated durations, up to 6300 s, the results showed negligible impact on NDSI.

15. SUBJECT TERMS
^dismount detection, hyperspectral imaging, normalized difference skin index, skin detection, spectral imaging

16. SECURITY CLASSIFICATION OF:			17. LIMITATION OF ABSTRACT	18. NUMBER OF PAGES	19a. NAME OF RESPONSIBLE PERSON
a. REPORT	b. ABSTRACT	c. THIS PAGE			Lt Col Jeffrey D. Clark, PhD (AFIT/ENG)
U	U	U	UU	94	19b. TELEPHONE NUMBER *(Include area code)* 937-255-3636 x4614 jeffrey.clark@afit.edu